Deposition of a Polydisperse Aerosol in the Upper Respiratory Tract

Fanny Bergman

DIVISION OF ERGONOMICS AND AEROSOL TECHNOLOGY
DEPARTMENT OF DESIGN SCIENCES
FACULTY OF ENGINEERING LTH | LUND UNIVERSITY
2020

MASTER'S THESIS

Deposition of a Polydisperse Aerosol in the Upper Respiratory Tract

Design and Evaluation of an Experimental Setup for Measurement of Aerosol Deposition in Mouth-Throat Models

Fanny Bergman

LUND
UNIVERSITY

Deposition of a Polydisperse Aerosol in the Upper Respiratory Tract

Design and Evaluation of an Experimental Setup for Measurement of Aerosol Deposition in Mouth-Throat Models

Published by
Department of Design Sciences
Faculty of Engineering LTH, Lund University
P.O. Box 118, SE-221 00 Lund, Sweden

Subject: Aerosol Technology (MAMM05)
Division: Ergonomics and Aerosol Technology
Supervisor: Jonas Jakobsson
Co-supervisor: Per Bäckman
Examiner: Jenny Rissler

Abstract

Inhaled pharmaceuticals are commonly used in the treatment of respiratory disease. This method of administration has many advantages but also poses a problem with particles being lost before reaching the target site. Particle deposition in airways is mainly an effect of inertial impaction, gravitational settling and diffusion. What mechanism influences a particle the most depends on the particle aerodynamic diameter and its linear velocity through the airways. To understand the influence of these parameters on the particle deposition in upper airways, an experimental method has been developed and tested on three different airway geometries, represented by 3D-printed airway models, at three different volumetric flow rates (15, 30 and 60 l/min). Results showed an increase in deposition for increasing flow rates, which was expected as a consequence of increasing inertial impaction. The estimated deposited fraction correlated well to CFD modelling, but generating low variability data turned out to be challenging. This problem could be addressed by further development of the aerosol generation technique, as this factor turned out to have a large effect on the calculated deposited fraction.

Keywords: Aerosol, particle deposition, upper airways, inhalation measurements, polydisperse aerosol generation, mouth-throat model

Sammanfattning

Inhalerade läkemedel är vanliga vid behandling av symptom i luftvägarna. Denna administreringsmetod har många fördelar, men ett problem är att en stor andel av läkemedelspartiklarna går förlorade på väg mot sitt mål. Partikeldeposition i luftvägar beror till stor del på impaktion, sedimentation och diffusion. Via vilken mekanism aerosolen deponerar beror bland annat på partikelns storlek och med vilken hastighet den färdas genom luftvägarna. För att förstå hur dessa parametrar påverkar partikeldeposition i de övre luftvägarna har en experimentiell metod utvecklats. Metoden testades för tre olika luftvägsgeometrier, representerade av 3D-printade luftvägsmodeller, för tre olika volumetriska flödeshastigheter (15, 30 och 60 l/min). Resultatet visade på en ökning av deponerad andel för högre flöden, vilket var en väntad effekt till följd av högre impaktion. Den uppmätta deponerade andelen partiklar stämde väl överens med CFD-modellen, men det var utmananade att samla in data med låg varians. Detta problem skulle troligen minska drastiskt om metoden för partikelgenerering vidareutvecklades, då variation i den genererade aerosolkoncentrationen pekats ut som en stor felkälla.

Nyckelord: Aerosol, partikeldeponering, övre luftvägar, inhalationsmätning, aerosolgenerering, luftvägsmodell

Acknowledgements

This Master's Thesis was conducted at the division for Ergonomics and Aerosol Technology at the Faculty of Engineering at Lund University during the spring/summer of 2020. The project was performed in collaboration with Emmace Consulting with the common objective of developing, and subsequently evaluating, a setup for measuring deposition of micrometer-sized particles in several models of human airways.

The project would not have been possible without the incredible support from my primary supervisor Jonas Jakobsson, thank you! You taught me so much during this relatively short time. I would also like to express my gratitude towards Per Bäckman and Mårten Svensson at Emmace consulting for regular input throughout this project. Thank you Fotos Stylianou and Stavros Kassinos, University of Cyprus, for guidance in design of experiments and for the project idea. To Jenny Rissler, Anders Gudmundsson, Jakob Löndahl and all others at EAT - thank you for sharing your knowledge and all good advice. Thank you Josef Forslund and the team at the IKDC workshop for the effort you put into making the mouth-throat model connections tighter and sturdier than I thought possible. Johan Wirén, Humle Design, thank you for ultra-fast 3D-printing even during Covid-19 crisis. To Rebecca Johansson for daily company and good discussions both in the office, lab and during lunch. The warmest thanks also to Lukas, family and friends.

Lund, September 2020
Fanny Bergman

Contents

List of abbreviations and symbols

APS	aerodynamic particle sizer
CFD	computational fluid dynamics
CMAD	count median aerodynamic diameter
COPD	chronic obstructive pulmonary disease
DF	deposited/deposition fraction
GSD	geometric standard deviation
MMAD	mass median aerodynamic diameter
MT	mouth-throat
NGI	next generation impactor
RF	recovered fraction
TOF	time-of-flight

B	particle mobility
C	particle concentration
d	tube diameter
d_a	aerodynamic diameter
d_g	geometric mean diameter
d_i	midpoint particle diameter of ith group
d_p	particle diameter
g	gravitational acceleration
m	mass
N	number of particles
Q	flow rate
Re	Reynold's number
S	stopping distance
Stk	Stoke's number
U_p	gas velocity in sampling probe
U_0	free gas velocity
η	gas dynamic viscosity
θ	angle of deviation from free gas stream
ρ_p	particle density
ρ_0	standard density
τ	relaxation time

1 Introduction

In 2015 over 3 million people died in chronic obstructive pulmonary disease (COPD), making it the third leading cause of death worldwide [Wang et al., 2016]. Treatment for respiratory disease, including COPD and asthma, is commonly administered through inhalation of aerosols. By means of inhalation the pharmaceutical product is directly delivered to its target in the lung, resulting in both rapid onset and less systemic side effects. This gives inhalation potential advantages when compared to for example orally administrated drugs. However, for the inhaled drug to reach the lung it must first pass the upper respiratory tract. Only a small fraction, at times estimated to be as low as 10-20 %, of the inhaled drug can accomplish this and reach the lung target. Particle size highly affects this deposition-dependent bioavailability of inhaled drugs, with small diameter aerosols depositing more peripherally compared to larger [Labiris and Dolovich, 2003]. Also the flow rate has an impact on the aerosol deposition, with higher flow rates resulting in more inertial impaction, which in turn leads to increased deposition of larger particles in the upper respiratory tract [Darquenne and Prisk, 2004].

Given the facts that inhaled aerosols deposits not only in the lung but also in the upper respiratory tract and that there is a high intra- and interindividual variation in the regional deposition [Golshahi et al., 2013, Heenan et al., 2004] understanding and predicting the therapeutic dose is difficult. *In vivo* studies on regional deposition of inhaled aerosols have been performed using scintigraphic methods. Such studies indeed gives valuable, patient-relevant, information but are expensive to perform and requires radio-labelled aerosols [Huang et al., 2020]. Because of this respiratory tract deposition has been studied extensively *in vitro* using either simplified geometries or replicas of human airways.

In vitro deposition studies have been performed using a broad range of methods including filters [DeHaan and Finlay, 2001, Delvadia et al., 2012], Andersen cascade impactors [Longest et al., 2009, Worth Longest and Hindle, 2009, Burnell et al., 2007], expansion balloons [Fadl et al., 2007] and an APS [Golshahi et al., 2013] to name a few. Studies like these have the advantage of being less complicated, not requiring human volunteers and allows better control over inhalatory flow rates and administered aerosols. However no such method has yet been approved by regulatory instances due to the current lack of sufficient data on the *in vivo* - *in vitro* correlations. To increase the understanding of *in vivo* - *in vitro* correlations several computational fluid dynamics (CFD) models have been developed. To be able to use such an *in silico* model in predicting the delivered dose in a subject that have not been studied experimentally the CFD model first have to be validated against an experimental data set [Byron et al., 2010, Huang et al., 2020]. The aim of this project is to generate deposition data for validation of a CFD model, described in detail in [Stylianou et al., 2017], aiding in the development of more efficient inhalation-solutions in the future.

The **primary objective** of this project is to develop a setup for measuring particle deposition of micrometer-sized aerosol particles in models of human airways during constant flow. A **second objective** is to evaluate the setup on physical models of human airways in a standard configuration (straight posture and inlet aerosol plume parallel to the horizontal plane) at a standard flow rate (60 l/min). The airway models have been re-constructed from magnetic resonance imaging (MRI) of a human subject in different postures and 3D-printed [Stylianou et al., 2017]. In total there are 9 airway models available, each representing a

different airway geometry and/or a different angle of the inlet aerosol plume in relation to the horizontal plane. A **third objective** of the project is to investigate how subject position and aerosol plume angle (represented by the different models) influence deposition in the upper airway models at different flow rates (15, 30 and 60 l/min).

This report introduces the reader to aerosol measurements in the upper respiratory tract with main focus on polydisperse aerosols in the size range 1-10 μm. The background, section 2, gives an overview on aerosol generation as well as common measurement techniques and their related difficulties. The reader is also introduced to the concept of aerosol deposition in the human respiratory tract. In the methods, section 3, the setup developed and used in this project is presented. The setup includes both a system for aerosol generation and a method to measure aerosol deposition in MT models. The results, section 4, from these measurements and recommendations for improving the setup are presented and discussed in the end of the report.

2 Background

2.1 Aerosol Generation

An aerosol is a particle suspension in gas which may have both natural and anthropogenic origin. Natural aerosols includes fog and ocean salt spray while aerosols such as smoke and inhaled pharmaceuticals are examples of anthropogenic aerosols. Throughout this report the word particles will be used to describe the non-gas phase of an aerosol, these particles may consist of either (or both) a solid or liquid form depending on the specific aerosol.

There are many techniques for technical generation of aerosols, but only the most common methods will be presented herein. In general, aerosols can be formed either by fragmentation and dispersion or by condensation. The technique chosen for a specified application depends on the concentration and aerosol characteristics needed. Aerosols with a wide size distribution are referred to as polydisperse while aerosols containing particles in a narrow size range are monodisperse. Whether an aerosol is considered mono- or polydisperse is determined by its geometric standard deviation (GSD), as described in section 2.3.

Atomisation is a method where a liquid is dispersed into gas-suspended droplets. Atomisation can be performed in several ways, the simplest form is hydraulic atomisation. The energy from pressurising a liquid is utilised in the form of kinetic energy to form droplets, either through formation of a jet or via a spinning nozzle. Pneumatic atomisers, also called nebulisers, produces small droplets via compressed air acting on a liquid and are the most common devices for technical production of aerosols. Other variations of nebulisers based on ultrasonic waves or spray cans, containing a mixture of the material and a propellant with high vapour pressure, are also available. Solid particle pharmaceutical aerosols can be produced using pressurized metered dose inhalers (pMDI's), by disssolving a solid material into a volatile solvent that evaporates following droplet formation.

In aerosol physics applications the most common method to generate solid particle aerosols is dispersion of dry powders. The powder is then fed into a generator at a constant rate. Inside the generator an aerosol plume is formed pneumatically. Using dry powders can cause problems with electrostatic charge build-up due to contact with inner surfaces of the generator. The charged particles will adhere to the walls of the generator in a manner that

is not stable over time, causing fluctuations in output aerosol concentration. The resulting aerosol may be discharged by letting it pass through a reservoir containing an ion-producing radioactive source.

Aerosols can also be generated by condensation of vapours. For condensation to occur in a predictable manner high control of condensation nuclei is required. When nuclei are controlled and condensation occurs slowly, the outcome is a quite monodisperse aerosol [Hinds, 1999].

2.2 Aerosol Deposition in the Respiratory Tract

2.2.1 Physiology of the Human Respiratory Tract

The human respiratory system consists of several functional units. Together all the functional units help leading oxygen-rich air into the lungs for exchange with the blood and allows carbon dioxide and other volatile compounds to be ventilated out of the circulation. Air is inhaled via the nose and/or mouth and passes through pharynx and further down into the larynx. These parts of the respiratory system are commonly referred to as the upper- or extrathoracic airways. The inhaled air next passes on from the larynx into the tracheobronchial compartment, consisting of a long tube, the trachea, dividing into two branching tubes, the bronchi. Each bronchus leads further into the lung while branching several times. The bronchi have rings of cartilage for support, this is what distinguishes them from the bronchioles further down the conducting zone. The bronchioles guides the air into what is known as the respiratory zone, this is where the blood-gas exchange takes place. Along the walls, and particularly at the distal end, of the respiratory bronchioles there are hollow sacs known as alveoli. The alveoli are in close contact with a rich net of capillaries which allows the gas exchange to take place [Widmaier et al., 2014, ICRP, 1994] A schematic representation of the respiratory tract can be seen in Figure 1.

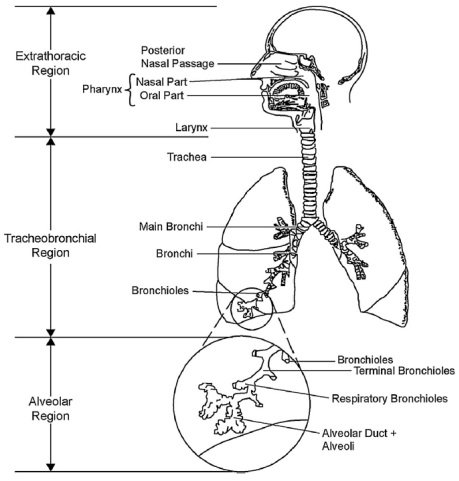

Figure 1: Representation of human respiratory tract as seen in [Brown, 2015].

As air flows down the respiratory tract during inhalation humidity increases, and at the level of the lung it is close to saturation. This humidity gradient is essential for airway function, but can also affect inhaled aerosols. Inhaled water dissolved drug formulations often

form hygroscopic aerosols, meaning that particle size may either increase or decrease when passing through the airways depending on the aerosol physico-chemical properties. Fine particles, $< 1\mu$m in diameter, may increase up to five times their initial size. It is important to consider hygroscopic effects when studying aerosols in the respiratory tract since it affects both deposition and the aerosol size distribution [Labiris and Dolovich, 2003].

2.2.2 Aerosol Deposition

The deposited fraction, DF, is an important measure to relate the inhaled dose to the dose available for biological interaction inside the body. This holds true regardless if the aim is to study inhaled pharmaceutical formulations, air pollution or other airborne particles. Deposition of inhaled aerosols is mainly an effect of inertial impaction, gravitational settling (sedimentation) and diffusion. The deposition mechanism of any given aerosol is highly dependent on particle size. Large particles, in the range of a few μm, are commonly deposited by inertial impaction during drastic changes in the direction of the air flow, particularly in the upper respiratory tract. Gravitational settling is more common for particles < 3 μm in diameter that reaches the alveoles and bronchioles, here the air flow is slower and the particles reside longer, giving them the time needed to settle. For diffusion to occur particle diameter need to be small, generally below 0.3 μm [Löndahl et al., 2014, Hinds, 1999]. Under certain rare conditions, while studying ultrafine particle deposition, the effect of particle charge may become relevant [Melandri et al., 1983]. For special cases, such as long fibers in small airways, interception may become relevant as well. During interception the particle will not deviate from the streamline, but deposits when close to a surface due to its size [Hinds, 1999].

The size-dependent regional deposition is described visually, for an average human breathing through the mouth, in Figure 2. The ICRP data [ICRP, 1994], presented in the figure, is commonly used for modelling purposes but it should be noted that it is semi-empirical. For this project only data in the particle size interval 1-10 μm (white background in the figure) is relevant. As seen from the figure, the main part of large particles deposit in the extrathoracic airways. Deposition in the extrathoracic airways, the mouth-throat region, is dominated by inertial impaction. This correlation has been found by plotting experimentally determined deposited fractions to what is known as the inertial impaction parameter, $\rho d_p^2 Q$. Here ρ is the particle density, d_p is the mass median diameter and Q the flow rate [Grgic et al., 2004].

The DF was throughout this project calculated as in Equation 1 [Heyder, 1975]. N denotes particle number and t time. Due to practical reasons the recovered fraction (RF) after a certain time is measured but it is readily correlated to the deposited fraction as $RF + DF = 1$ in an enclosed system.

$$DF = \frac{N(t_1) - N(t_2)}{N(t_1)} \tag{1}$$

The physical conditions during which a particle deposits is also of interest in aerosol measurements. Once the resistive drag force, due to viscosity when the particle travels through a gas, equals the gravitational force the particle is said to have reached its terminal settling velocity. The terminal settling velocity can be expressed as in Equation 2 where V_s is the terminal settling velocity, ρ_p the particle density, g gravitational acceleration and η the dynamic viscosity of the gas [Baron et al., 2011, Darquenne, 2012]. This particle property

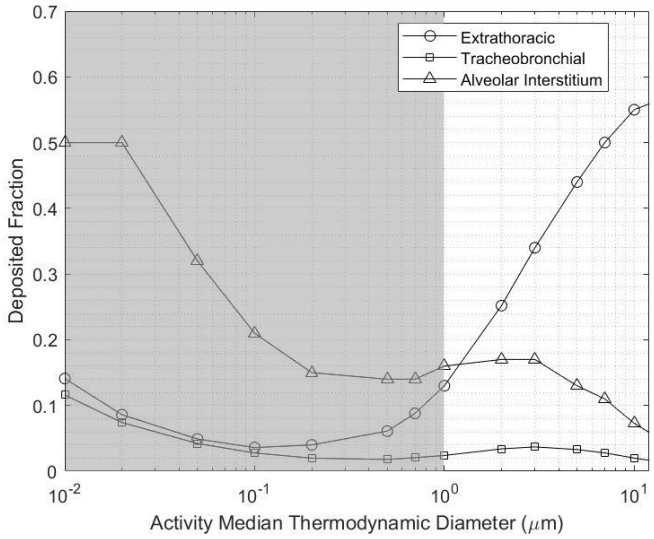

Figure 2: Deposited fraction in the respiratory tract as a function of particle diameter for a human breathing through the mouth. The particle range of interest for this work is showed with light background. As seen in the figure the deposition of larger particles is significant in the extrathoracic region. Data from [ICRP, 1994]

will be used later on to define the aerodynamic diameter, needed to compare non-spherical particles or particles of varying density.

$$V_s = \frac{\rho_p d_p^2 g}{18\eta} \tag{2}$$

Deposition in the respiratory tract depends not only on aerosol properties and physiological structure, but also on the breathing pattern, i.e. the flow rate and breathing frequency [Heyder et al., 1986, Taulbee and Yu, 1975]. The route of breathing, through the mouth or nose, also affects the amount of particles penetrating into the lung. This is because our nasal cavity is more efficient in removing particles compared to the oral counterpart [Brown, 2015]. For pharmaceutical aerosols the inhalation device of choice have an effect on aerosol deposition in the extrathoracic region, with the highest deposition observed for dry powder inhalers [DeHaan and Finlay, 2001]. The local deposition of aerosol also varies not only between [Golshahi et al., 2013, Borgström et al., 2006], but also within individuals. By studying local velocities and deposition in realistic extrathoracic models (created from MRI scans) [Heenan et al., 2004] found significant differences from altering the position of the subject's tongue. In conclusion it should be stressed that the problem is not necessarily that some aerosols deposits in the upper airways but rather that it varies, thus creating uncertainties with regard to the therapeutic dose.

2.3 Particle Data

As particle size affects the properties of a given aerosol, a reliable way to measure the size of individual particles is of high importance in aerosol science. To account for particles of irregular geometry, and allow comparison, the concept of aerodynamic diameter is commonly used. The aerodynamic diameter of a particle is defined as equivalent to the diameter of a spherical particle of unit density that has the same settling velocity as the particle.

Most aerosols show a skewed distribution function, with a long tail for large particles. Because of this a lognormal distribution function is usually a better fit to experimental data. Such a distribution is usually described using the median aerodynamic diameter (MAD), the diameter at which half of the particles in the distribution are smaller and the other half is larger. The equivalent of the standard deviation for lognormal distributions is the geometric standard deviation (GSD), defined below. The GSD is always ≥ 1 [Hinds, 1999].

$$\text{GSD} = e^{\left(\frac{\sum n_i(\ln d_i - \ln d_g)^2}{N-1}\right)^{1/2}} \quad (3)$$

Where n_i is the number of particles in the ith size group, d_i midpoint particle diameter of the ith group, d_g is the geometric mean diameter and N total number of particles. The GSD can be used to describe whether a given aerosol is considered mono- or polydisperse. If the GSD > 1.15 the aerosol is referred to as polydisperse [Brown, 2015]. The aerosol size distribution is commonly plotted with the aerodynamic diameter on the logarithmic x-axis and the unit $dn/dlogD_p$ on the y-axis. $dn/dlogD_p$ takes the particle concentration in each group (dn) and normalises it to account for differences in sampling instrument resolution by division with the logarithm of the channel width, $dlogD_p$.

2.4 Characterizing the Aerodynamic Size Distribution of an Aerosol

There are a number of methods to detect and determine the size distribution of a given aerosol. This section will introduce the most common measurement instruments with a focus on the aerodynamic particle sizer (APS) used during this project. The APS was the obvious option due to easy operation, direct measurement of concentration for each particle size and, perhaps most important, its ability to detect particles in the entire (size) range of interest. The APS also have a temporal resolution that is high enough to detect particle deposition, even if aerosol concentration is not perfectly constant.

2.4.1 Potential Methods

Aerosols can be captured using sampling filters for later analysis. This type of collection approach is also used in impactors, analytical devices able to not only collect particles but also separate them into different size fractions. This is achieved by dragging air through a device with sharp turns, inertia will then cause particles above a critical size to impact on the surface. This is commonly performed in several steps, dividing particles into size groups for later analysis. Another device that can be used to separate large particles from an aerosol is the cyclone. In a cyclone the air moves in a spiral pattern, depositing particles due to the centrifugal force.

When it comes to direct measurement methods there is also a wide range of options to choose from, and the ones presented here are just a few examples. Optical particle counters uses detection of, commonly monochromatic, light scattering to determine concentration and size of aerosol particles. Many scattering angles are measured resulting in a final electrical signal by computational transformation. Optical particle counters are not suitable for small particles, below ≈ 300 nm, in this range condensation particle counters are preferred. Inside a condensation particle counter the aerosol particles flow through a saturated vapour, the particles act as nucleation centres for vapour condensation. This cause the particles to grow and allows scatter detection. Charged particles can be classified by their electrical mobility in a differential mobility analyser. The condensation particle counter and differential mobility analyser can be combined, forming together a scanning mobility particle spectrometer (SMPS) [Baron et al., 2011].

2.4.2 Aerodynamic Particle Sizer

The aerosol size distribution was measured with an aerodynamic particle sizer (APS) throughout this project. The main components of an APS 3321 (TSI) are shown in Figure 3. The aerosol is accelerated in a tube surrounded with a (higher) sheath flow inside the APS. At the end of the tube the aerosol is forced through a nozzle, increasing the velocity. The sheath flow focuses the aerosol stream into a narrow jet that passes through two laser beams. When a particle passes through the laser beam light is scattered, this scattered light is detected and converted into an electrical signal by a photo-multiplier tube or a semiconductor photo-diode. Once the particle passes through the second beam, another electrical pulse is generated. The time-of-flight (TOF) between the two signals can be used to calculate the average velocity of the particle. This velocity is related to particle size, as larger (and heavier) particles are not as easy to accelerate as lighter. By calibrating the instrument the TOF for a particle of a certain size can thus be related to its (aerodynamic) diameter [Hinds, 1999, TSI, 2012]. While the APS detects single particles as counts, represented by the number concentration, the instrument can readily convert this number to an area or volume (mass) measurement. The maximum concentration that can be detected using an APS without risking coincidence in the detection zone is 1000 particles/cm^3.

APS units are generally good at determining the aerodynamic diameter, however the counting efficiency, the concentration measurement of the instrument, have previously been a subject of high variation. Thanks to product upgrades this is less of a problem today. The counting efficiency of the APS mainly depends on the aspiration, that is the ability of the instrument to collect the aerosol, and the transmission through the APS unit. Apart from these flow-properties an efficient sensor is required to achieve correct counts from the scattered laser beam. Solid mono-disperse particle aerosols have been shown to be detected efficiently by the APS 3321 in the range from 0.8 to 10 μm. Contrary, liquid particles tend to show a decreased counting efficiency for increasing particle size. This effect can partially be explained by loss in the inner sampling nozzle [Volckens and Peters, 2005, Baron et al., 2011].

In a study including four APS instruments the intra-unit variation of APS 3321 when measuring monodisperse polystyrene latex spheres was found to be small. Inter-unit variation in number concentration, represented by the coefficient of variation, was also small, whereas the inter-unit variation for mass concentration differs significantly between instruments [Volckens and Peters, 2005]. In a more recent comparison of 15 APS 3321 units the

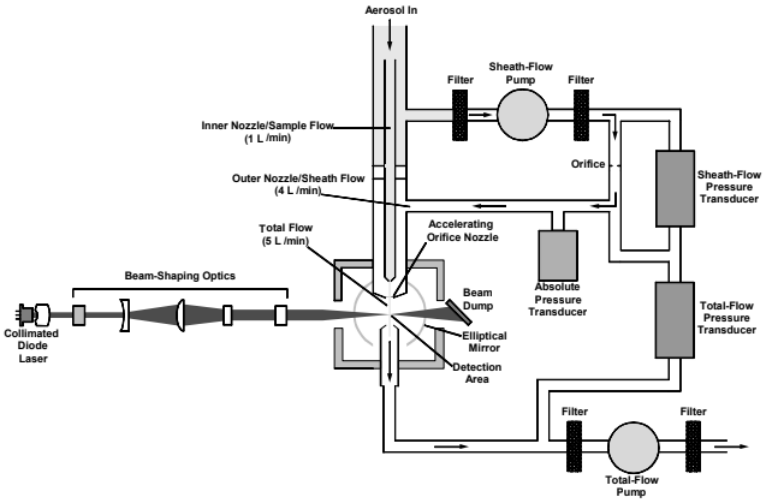

Figure 3: Simplified sketch of APS model 3321 from [TSI, 2012].

inter-unit variation was found to be higher. In the diameter range of 0.9-3 μm the relative deviation was approximately 10-20 %, while larger particles had estimated deviations between 40 and 130 %. However, counting statistics in the upper range was poor in this study, which makes any conclusions from the large particle data uncertain [Pfeifer et al., 2016]. Concerning mass estimations APS 3321 seem to underestimate the particle concentration when compared to a cascade impactor. However, the shape of the particle size distribution is consistent with impactor measurements [Peters and Leith, 2003].

2.5 Impact of Sampling Conditions

Whether a gas flow is laminar or turbulent depends on the relation of inertial and viscous forces in the system. The ratio of inertial to viscous forces is known as Reynolds number, Re, and is given in Equation 4. ρ is the density of the gas, U_0 is the gas velocity, d the diameter of the gas-containing tube and η the dynamic gas viscosity. The gas flow is laminar when Re < 2000 [Baron et al., 2011].

$$Re = \frac{\rho U_0 d}{\eta} \tag{4}$$

If flow conditions change, for example when the gas reaches an angled bend, the aerosol particles will adapt to the new conditions. However, this adaptation takes a certain time (distance), and the ratio of the stopping distance, S, to a characteristic dimension such as a tube diameter, d, is known as Stokes number or Stk, Equation 5. Here τ is the relaxation time of the particle and depends on particle mass and mobility, Equation 6. U_0 is the free air velocity and d_c the cylinder diameter. When Stk >> 1 particles will continue travelling linearly as gas flow bends, while if Stk << 1 particles follows the gas streamlines as they bend. Stokes number is a useful definition since it relates to the amount of particle inertial impaction [Hinds, 1999].

$$Stk = \frac{S}{d} = \frac{\tau U_0}{d} \tag{5}$$

$$\tau = mB = \frac{\rho_0 d_a^2}{18\eta} \tag{6}$$

τ thus depends on the particle mass, m, and mechanical mobility, B. ρ_0 is the standard density, d_a the aerodynamic diameter and η the dynamic viscosity of the carrier gas. Through Equation 5 and 6 it becomes clear that particles with larger aerodynamic diameter have a greater Stokes number and are subject to more inertial impaction. The same is true for higher particle velocities (U_0), a higher flow rate increases the probability that a particle of a certain size will deviate from the flow streamlines at, for example, a bend.

During experimental sampling it is important to make sure that the collected data is representative of the aerosol measured. This is achieved through isokinetic sampling conditions, where the sampling probe is aligned with the streamlines of the gas, and the gas velocity in the probe inlet is equal to the velocity of the surrounding gas. In practice this implies that the diameters for the sampling probe and an aerosol travelling in a cylindrical object follows the relationship established in Equation 7. Q_p being the flow rate of the sampling probe, Q_0 the flow rate of the gas in the cylindrical geometry, D_p the sampling probe diameter and D_0 the diameter of the cylindrical geometry [Hinds, 1999].

$$\frac{Q_p}{Q_0} = \left(\frac{D_p}{D_0}\right)^2 \tag{7}$$

Failure to sample isokinetically can be the result of two main causes; either the flow rates are mismatched or the sampling probe is not aligned with the gas volume. If U_p is the gas velocity in the probe and U_0 the velocity of the freely moving gas in the cylindrical duct, the result of $U_p < U_0$, known as sub-isokinetic sampling, will be that small particles follow the stream lines of the free gas (short relaxation time and thus lower Stk), they are simply swept past the sampling probe. The consequence of this is over-estimation of large particles, avoiding the curvilinear motion of smaller particles escaping detection. The opposite case is super-isokinetic sampling, $U_p > U_0$, during which large particles will not be estimated correctly due to their higher inertia and accompanying failure to follow the stream lines into the tube as smaller particles does. This shifts the particle size distribution towards smaller particles [Hinds, 1999, Welker, 2012].

When the sampling probe is not parallel to the free gas stream lines sampling is known as anisoaxial. Particles that have high enough inertia may cross the limiting streamline, giving

an aspiration efficiency $\neq 1$. There are empirical formulas to estimate the concentration error for any given value of Stk and angle of deviation, given that the sampling flow rate is isokinetic. However, when sampling is both anisoaxial and non-isokinetic the relationship becomes more complicated. When Stk > 6, and the angle of deviation from free gas streamlines is $0° \leq \theta \leq 90°$, the maximum concentration error can be estimated from Equation 8 [Hinds, 1999, Baron et al., 2011].

$$\frac{C}{C_0} = \frac{U_0}{U_p}\cos(\theta) \tag{8}$$

Depending on the aerosol of choice effects such as agglomeration/ aggregation, condensation and/or evaporation might need to be considered during sampling. Generally such measurement conditions are harder to characterise and results may be more difficult to interpret.

2.5.1 Transport loss during sampling

Even when sampling is performed isokinetically, and sampling efficiency is undistorted, particles will be lost during the aerosol transport to the measurement equipment. Transmission losses occur due to gravitational settling and impaction at sampling tube bends or as a consequence of turbulence. Apart from these factors particles can be lost due to the presence of electrostatic forces and thermal diffusion. Additional transmission losses occurs for anisoaxial sampling; when the aerosol enters the sampling probe particles will impact on the probe wall in the direction of the free stream flow.

To reduce losses the tubing system should be aimed at being as short as possible and not contain sharp angles. The system should also reduce turbulence as well as have a constant tube diameter. It is not uncommon that the sampled particle size distribution is unevenly distorted, and the sample fails to represent the true aerosol composition. This is particularly problematic for particles of large aerodynamic diameter, since they are subject to higher inertial and settling forces [Baron et al., 2011, Hinds, 1999]. When designing a measurement setup to study deposition it is important to consider sampling transport loss. If the fraction lost in the model inlet sampling line is not equal to the fraction lost in the outlet sampling line the calculated DF will be affected.

3 Methods

3.1 Aerosol Generation

The aerosol used in this project must cover the size range of interest, 1 to 10 μm, as well as be stable and reproducible during particle generation. It also preferably should be non-toxic and not damage sensitive sampling equipment or MT models. To determine a deposition fraction particles need to stick to the site of deposition. Most aerosols adhere to surfaces, and each other to form agglomerates, via van der Waals forces. Larger particles, above 0.1 μm often have a small net charge as well, allowing them to adhere to each other when in close contact via Coulomb forces. For liquid particles surface tension also adds on the ability to stick to surfaces. For solid particles however, the adhesion forces are not always large enough for particles to stick, and they may bounce at the surface. This may occur for high particle velocities (flows) and can be reduced by introducing a greasy film (coating) on the adhesion surface [Baron et al., 2011]. Since the rest of the measurement setup is partially dependent on the chosen aerosol, the aerosol generation method was determined first. Two different methods were evaluated; one creating liquid particles via condensation and the other produced solid particles by powder dispersion.

3.1.1 Fog Machine

The first aerosol generation technique tested was a fog machine for home-use (Velleman VDL800SMT2). The fog machine was filled with a smoke fluid (HQ Power VDLSL1) consisting of water mixed with glycols and mineral oils in unknown proportions. The fog machine was easy to operate and produced a non-toxic aerosol with liquid particles. The machine pumped the smoke fluid from a reservoir past a heating element, turning the liquid into gas. When the gas flowed out of the warm fog machine into the cool surrounding air it condensed, creating a thick fog. The fog machine was operated in a 22 m^3 test chamber in intervals of a few minutes. The TSI APS 3321 measured continuously during generation and dwell.

3.1.2 Dust Generator

The second aerosol generator tested was a powder disperser (Palas BEG 1000 S) fed with soda-lime glass microspheres (Potters Industries Spheriglass 5000). During the experiments the problem of hygroscopic particles was encountered. When measurements were performed on days with high ambient relative humidity the powder could not be sufficiently dispersed. This problem was solved by drying and sieving the powder before measuring. The powder was found to have an approximate moisture content of as high as 20 %. Dried powder was used only for 0 ° MT model in the final measurements.

Pressurised air was connected to the generator and the powder released, a little at a time by a transport belt and a rotating brush, into the airstream and a specialised ejector nozzle to create a polydisperse solid particle aerosol. The dust generator produced an aerosol that was lead into a 1 m^3 box. An APS sampling tube was also inserted into the box to give an initial estimation of the aerosol produced.

3.2 Measurement System Development

The general idea of the measurement setup was to create similar flow conditions at the model inlet and outlet, and measure aerosol size distributions using two APS units. Although not achieving fully isokinetic sampling the setup was designed to minimise anisokinetic effects. To minimise transport loss, the sample tubing was shortened as much as possible, and unnecessary sharp bends avoided. By sampling at two points in the setup data to calculate the DF (Equation 1) could be collected, assuming a relatively constant aerosol generation.

3.2.1 Mouth Throat Models

The measurement system needed to support all nine MT models, but only three models were measured during the project. The models had three different inhalation mouthpiece angles; 0, 15 and 30 ° upwards from a horizontal inlet orientation. These models in particular were chosen since the CFD model predicted the largest difference in DF between them. The inhalation mouthpiece used was a ≈10 cm long metal tube with 8 mm inner diameter, predetermined from the CFD modelling. The second model factor was the head orientation; head straight, up or left. In practice this meant that the inlet and outlet sampling points was not fixed in relation to each other when switching MT model. Figure 4, left, shows a cross sectional view of the standard model, head pointing straight forward and inhalation mouthpiece in horizontal position, this MT model was used for system design. All models were created from MRI scans of a male subject holding an inhaler mouthpiece between the lips. MRI data was processed into 3D-models that were printed to create a physical model that could be used for experiments [Stylianou et al., 2017].

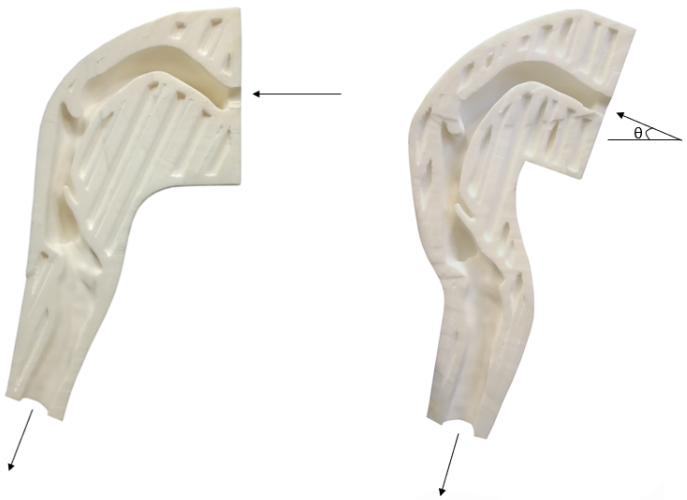

Figure 4: Cross sectional view of throat models. The arrows indicates the flow direction. The aerosol inlet pipe is inserted into the holes that the upper arrows are pointing towards. Left: 0 ° inclination, straight forward MT model. Right: MT model straight forward, $\theta = 30$ ° inhalator mouthpiece inclination.

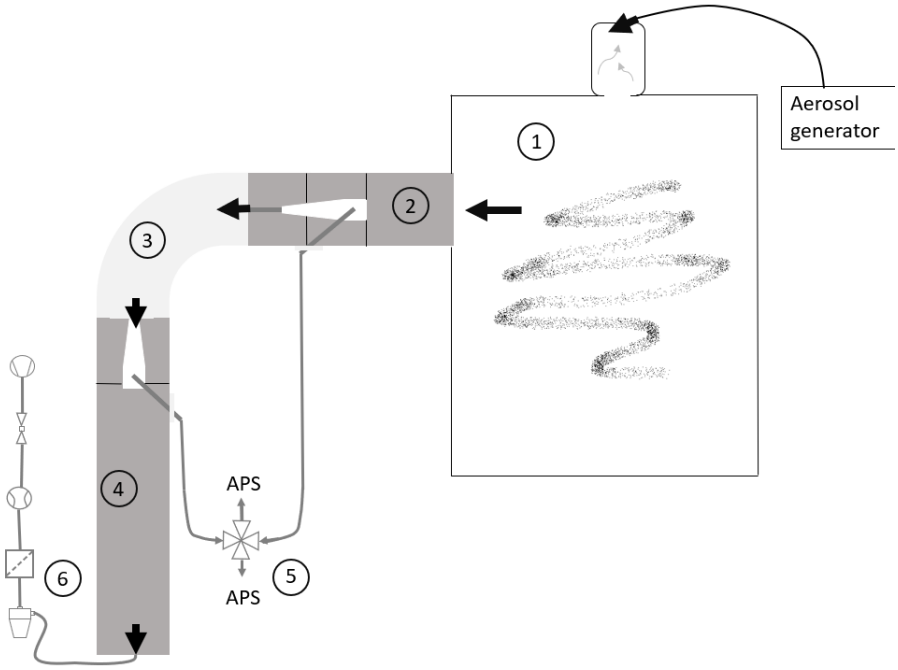

Figure 5: Experimental setup. (1) Aerosol reservoir. (2) Tube containing a funnel leading the aerosol into the MT model. Aerosol was sampled inside the funnel. (3) MT model (4) Outlet tube and funnel. Aerosol was sampled inside the funnel as it exits the model. (5) 4-way vent for sampling tube switch, connecting the aerosol inlet and outlet to two APS units. (6) Air exiting the second ventilation tube was filtered through a cyclone and a filter. The air flow was generated by the in house vacuum system and controlled via a valve and a flow meter.

3.2.2 Test System Setup

The MT model was placed with the inlet pipe in the horizontal plane for MT models without inclination angle. The aerosol flows through the model as indicated by the arrows in Figure 4, showing a cross sectional view of two of the MT models. The model (3) was placed in the centre of a tubing system as seen in Figure 5. Aerosol was forced through the tubing system and the MT model using a vacuum pump. The test aerosol was generated by the particle generator (Palas BEG 1000 S) and transported through a hose into a mixing volume of approximately 25 l. In the volume four tubes connected to a compressed air pump were inserted, creating turbulence. The mixing volume was placed on top of a 1 m^3 box (1). Inside the box air was further mixed by two table fans. The aerosol was drawn into the MT system through a 10 cm in diameter hole in the side of the box.

First the aerosol entered a horizontal 10 cm diameter 50 cm long ventilation tube (2) and flowed through a funnel-shaped container. By using the funnels both upstream and downstream the model it was possible to assure that the aerosol sampled at the inlet was representable for the aerosol entering the model and the aerosol sampled at the outlet was representable for the aerosol that has passed the model. Thus the funnel was sealed at the edges to avoid air passing on the sides. The funnels also served to modulate the linear gas velocity for the aerosol passing the model, and thus to achieve symmetrical flow conditions at both sides of the model. Without a funnel present there was a high risk of mixing at the

interface between the tube and the model as the inlet diameter changed the flow drastically. A sketch of the funnel and the sampling tubes is shown in Figure 6. The funnel was placed concentric in the ventilation tube by two supporting plastic discs with holes in the centre. The first disc was placed at the base of the funnel, sealing the inlet funnel to the tube. The second disc was placed approximately 10 cm away towards the pointy end. Also at the pointy end, the inlet pipe leading the aerosol into the MT model (3) was inserted into the funnel. O-ring seals ensured a tight fit between funnel and pipe, while a hose and a flat washer around the pipe ensured a constant distance and even pressure on the seal.

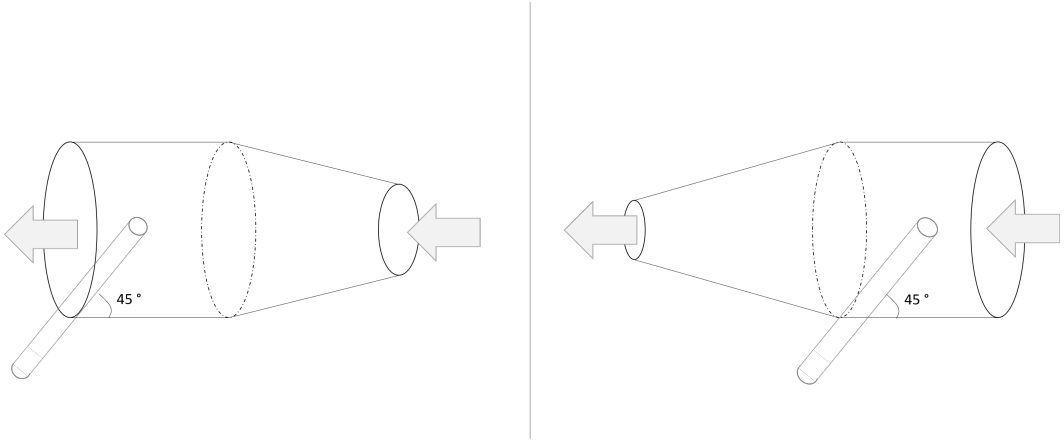

Figure 6: Funnel-shaped sampling volume with flow direction indicated by arrows. The sampling tube is inserted into the funnel in a 45 ° angle. Left: Outlet sampling funnel. Right: inlet sampling funnel.

The MT model was fixated at the inlet and outlet using custom made plastic adapters, Figure 7. The inlet adapter connected the mouth-part of the MT (3) (including the aerosol inlet pipe) to the horizontal tube (2) and allowed changing of MT model since it was secured by a tight fitting inner seal. The inlet adapter was glued and screwed onto a ventilation tube lid that could be slided onto the 10 cm tube and locked tight by a rubber seal.

At the outlet end the MT model was secured by a next generation impactor (NGI) connector. The NGI connector allowed easy switching between models. It was fitted inside the angled opening (5 °) of an outlet adapter, see Figure 7. The outlet adapter itself was glued and screwed tight on top of another ventilation tube lid. The aerosol flowed through the NGI connector and outlet adapter and entered the second, vertical, tube (4). The vertical ventilation tube had an approximate length of 1 meter, allowing outlet measurement to be performed with minimal influence from flow patterns created when air passes the constriction at the tube distal end. The second funnel was glued (using silicone) onto the inside of the tube lid with the pointy end towards the MT model and NGI connector. Also this funnel was secured using a plastic disc with a centred hole fitted around the base.

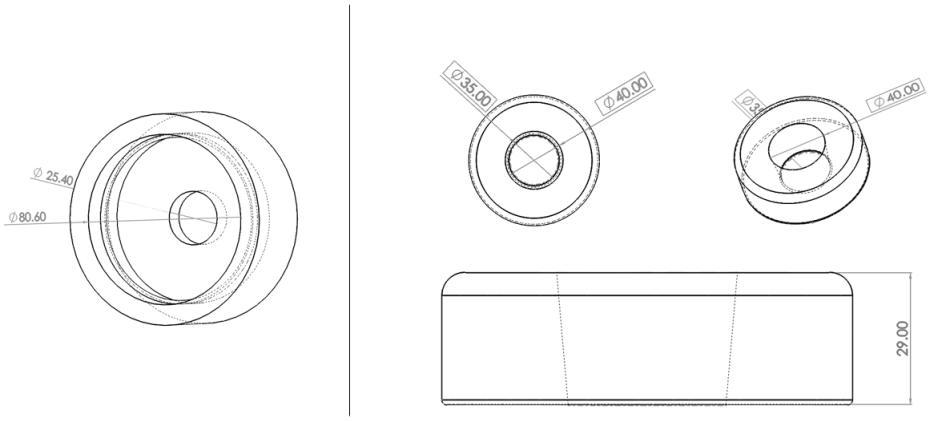

Figure 7: Drawings of inlet and outlet adapters. Left: Inlet adapter connecting the ventilation tube lid to the upper part of the MT model. Right: Outlet adapter, placed at the MT model end, surrounding the NGI connector.

Aerosol was sampled continuously at the model inlet (2) and outlet (4) of the MT model using two APS units (APS 3321, TSI). A sampling tube, inner diameter 50 mm, was inserted into the centre of the funnel on each side of the model in a 45 ° angle against the flow direction. By setting the angle to 45 ° the two sampling tubes, mounted at the horizontal and vertical tube, were parallel. Thus minimising the difference in particle loss due to impaction and sedimentation. Unfortunately, since the flow through the model varies and does not match the sampling flow velocity, estimating the error due to isoaxial sampling was not possible.

The 45 ° angle was fixated by a 3D-printed holder on the outside, seen in Figure 8. The 45 degree sampling tube was connected on the model inlet side (2) via a short piece of plastic hose to another steel tube that lead the sampled aerosol vertically approximately 30 cm and then through a smooth bend into a 4-way ball valve (Swagelok SS-45YF8). The sampling tube on the model outlet side was connected via a short plastic hose to another steel tube. This tube was also smoothly bent to enter the 4-way valve from the opposite side compared to the model inlet sampling tube. Two identical, twice curved to 45 °, steel tubes connected the two valve outlets to an APS unit on either side of the setup.

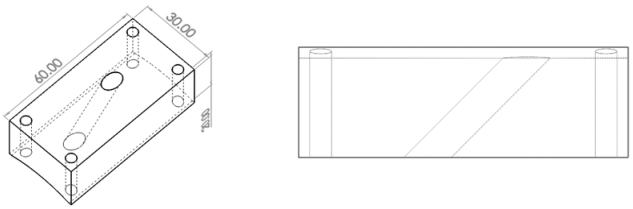

Figure 8: Drawing of 3D-printed part for keeping the sampling tube in a 45 ° angle. Printed twice and fastened at the ventilation tubes close to the model inlet and outlet.

At the end of the vertical ventilation tube (4) a vacuum tube was connected through the lid. The tube lead the aerosol that exited the model through a cyclone, removing large particles, and next through a particle filter (6). The filtered air passed through a flow meter (TSI 4043 thermal mass flow meter). Flow was regulated by a plug valve (NUPRO SS-8P6T4-RT) placed before the vacuum pump in the flow direction.

The flow inside the funnel sampling volume was found to be laminar, see Equation 4, for all flow rates (15, 30 and 60 l/min). Table 1 indicates that there is a difference in the linear flow velocity between the APS sampling tube and the funnel where sampling is performed for all flow rates measured. For isokinetic sampling the linear flow velocity should be equal to the flow velocity in the funnel and the sampling probe aligned with the flow direction. In this setup this is not fulfilled. From the table it becomes clear that 15 l/min gives the least representative sampling while 60 l/min is still not optimal but considerably closer to the sampling flow velocity. Still the conditions should be similar at the model inlet and outlet.

Table 1: Volumetric flow rates used during the measurements and their corresponding linear flow velocities. The geometry column gives information on what part of the system the calculation is valid for.

Volumetric flow rate (l/min)	Geometry	Linear flow velocity (m/s)
1	APS sampling tube	0.85
15	Funnel	0.10
30	Funnel	0.21
60	Funnel	0.42

3.3 System Characterisation

System characterisation includes all measurements performed to ensure that the measurement setup was functional. The only MT model used in this section was the standard, 0 ° inclination and straight forward, model. All data presented for system characterisation in the results are unfiltered and should be regarded as development data, not final measurements.

3.3.1 Stability Measurement

Aerosol generation stability was tested with the standard MT model, no inhalator angle and head straight forward. Both APS units were connected to the sampling point at the MT model inlet (2) via a Y-connector. The outlet sampling point (4) was plugged. Figure 9 shows the stability measurement setup. The aerosol generator was started approximately 30 minutes before the measurement started. The flow through the MT model was 30, 60 and 90 l/min. Data was recorded during one hour per flow condition.

3.3.2 Coating Influence

The need of coating was tested by first measuring DF in the uncoated standard model for flows of 15, 60 and 90 l/min. Sampling time was 30 s and measurement time 5+1 min (data collection + time for switching). The APS unit measuring at the inlet/outlet was switched 5 times for each flow, resulting in a total measurement time of 30 minutes per flow. The model was next coated with silicone spray. The spray was applied to both inlet and outlet and allowed to deposit on all inner surfaces before being dried by blowing compressed air through the MT model. DF measurements were repeated for 15, 60 and 90 l/min with the MT model being recoated for each flow.

3.3.3 Repeatability Measurement

Repeatability was tested for flows of 15, 60 and 90 l/min through the standard model. Sampling time was 30 s and measurement time 5+1 min (data collection + time for switching). The APS unit measuring at the inlet/outlet was switched 5 times for each flow, resulting in a total measurement time of 30 minutes per flow. Measurements were repeated three times on different days and the model was dismounted, cleaned with water and compressed air and recoated after each measurement day.

3.3.4 System Particle Loss Measurement

Particle loss due to impaction and gravitational settling in the system was practically inevitable in the particle range of 1 to 10 μm and for high aerosol flow rates. To estimate particle loss in the system, the MT model, (3) in Figure 5, was replaced by a 25 cm long flexible, antistatic hose with inner diameter 25 mm. The hose was bent to an angle of approximately 45 degrees in relation to the flow direction and inserted between (2) and (4). One end of the hose was inserted into the NGI connector and the other end slided onto a quick connect coupling. The quick connector had an inner diameter of 16 mm at the end connected to the hose. The other end of the connector had an inner diameter of 10 mm, onto which a 10 mm long hose with a 16 mm diameter was slided. The hose was secured around the pointy end of the funnel at the inlet sampling point. The particle loss setup is shown in Figure 9. System particle loss was measured with 15, 30, and 60 l/min flow through the system. Sampling time was 30 s and measurement time 5+1 min (data collection + time for switching). The APS unit measuring at the inlet/outlet was switched 5 times for each flow, resulting in a total measurement time of 30 minutes per flow.

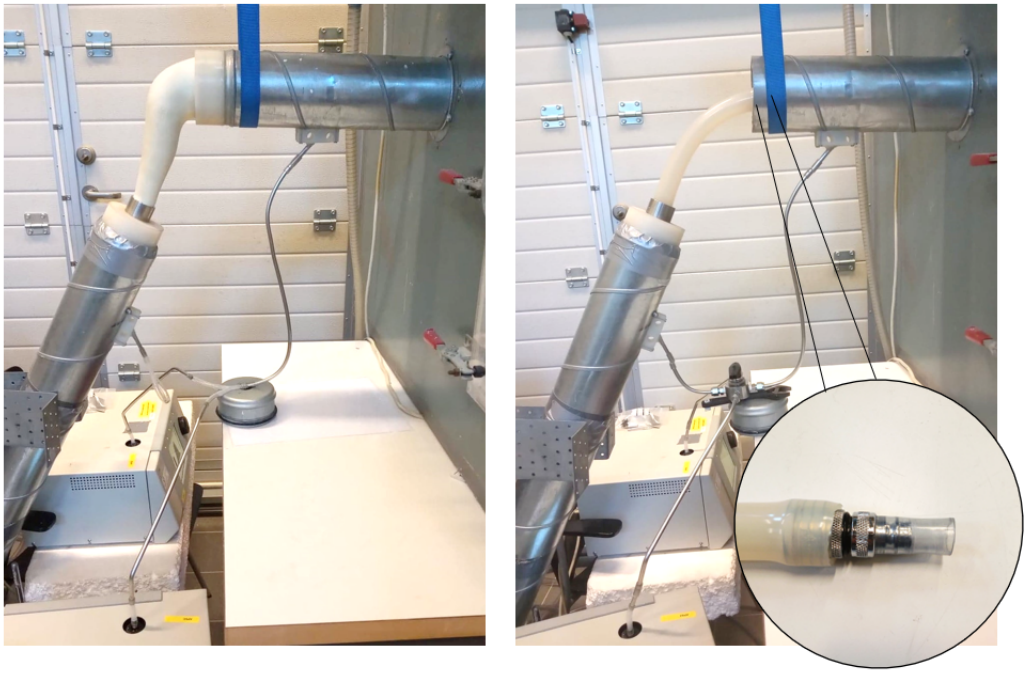

Figure 9: Left: Setup used during aerosol stability measurement. Both APS units were connected to the inlet sampling point via a Y-connector. Right: Setup for measuring system particle loss, a hose was used to replace the MT model. The inset shows the end of the hose connecting to the funnel (2).

Particle loss in the sampling tubes was measured by placing both APS units underneath the aerosol mixing box. The sampling tubes (both model inlet and outlet part) were inserted into the box through a hole in the floor. Two vertical tubes of the same diameter were inserted through the bottom as well. Both APS units measured through the vertical tubes for 30 minutes to establish a baseline concentration with minimal sampling tube loss (hence the short vertical tubes). The bent sampling tubes, including the valve, were next connected to each APS. The flow through the tube was 1 l/min, the APS aerosol flow rate. The valve was switched five times with a five minute measurement for each period. Sampling tubes were then switched back to the initial vertical tubing and both APS units sampled for 30 minutes. From this data an average DF for the inlet and outlet sampling tube was calculated.

3.4 Final MT Model Measurements

MT models with three different inclination angles (0, 15 and 30 °) were mounted in the measurement setup as seen in Figure 10. The remaining six MT models (representing head turning and combination effects from inclination angle) were omitted from the final measurement procedure due to time limitations. For measurement on 15 ° inclination model the sampling tubing was extended by a 4 cm long identical tube connecting to the APS on each side. The sampling tube at the MT model outlet was also extended by a 4 cm long tube. For the 30 ° inclination model the APS connection tubing was extended with 13 cm on each side, compared to the standard model. The outlet sampling tube was extended 8 cm, see Figure 10.

DF was measured for flows of 15, 30 and 60 l/min for each of the three models. APS sampling flow was switched five times for each flow rate through the model, resulting in a total data collection of 3∗5 minutes before and 3∗5 minutes after the MT models for each APS. Each model was dismounted, cleaned with pressurised air and water, and recoated between each flow rate.

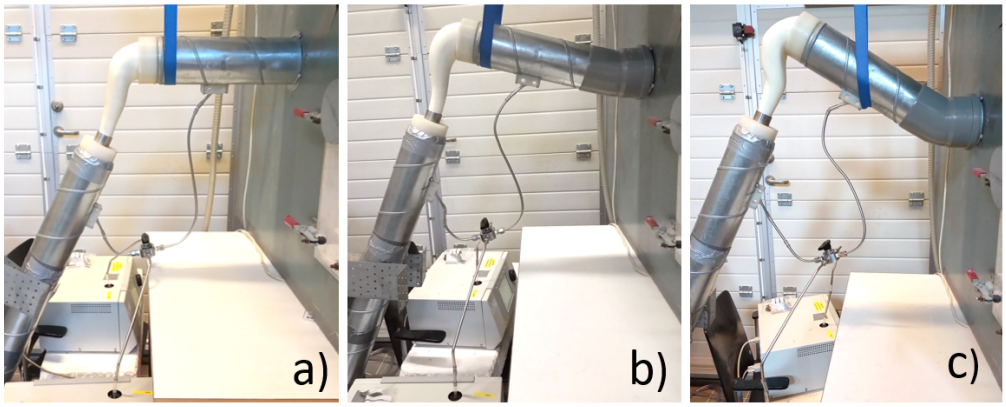

Figure 10: MT models with varying inclination angle mounted in measurement setup. a) No inclination angle b) 15 ° inclination c) 30 ° inclination.

3.5 Data Treatment

The APS main output was a vector of particle counts for particles belonging to a certain size bin. These size bins were unequally distributed, so that the bin width is narrower for small particle diameters and wider for larger size bins. For each size bin the DF, Equation 1, was calculated using a MATLAB script. Data collected one minute after each sampling flow switch was automatically discarded before performing the calculation. DF was calculated from a mean of 3x10 samples measured at the model inlet and 3x10 samples measured at the model outlet where each sample was 30 s long. Two samples (30 s each) was discarded for each switching event.

For the final MT model measurements filtered data, see section 3.5.1, was plotted together with the deposited fractions as calculated by the CFD model. Deposition mechanisms accounted for by the CFD model was inertial and gravitational forces. For details on modelling see [Stylianou et al., 2017].

3.5.1 Filtering

During system characterisation measurement DF was calculated regardless if there was a significant difference in concentration. The reasoning behind this is that this data was only generated to develop and characterise the measurement system, not to study deposition as such. In the final MT model measurements data was filtered to reduce noise. The need for data filtering was found from measurements such as the ones shown in Figure 16 and 17, where, as described in results section, there was a low signal to noise ratio mainly for small particles. In the final MT model results DF was only plotted if there was at least a $2*$ Std difference between the model inlet (high) and model outlet (low) level for each size bin and individual APS. The $2*Std$ was deemed to be a reasonable threshold value for level of quantification. The standard deviation per size bin used in this filtering was calculated as the average standard deviation during the three hour stability measurement (aerosol generation stability), see also section 4.2.1. Data from the stability measurement was used since it only contains samples at the model inlet, and thus is more representative of aerosol generation and its accompanying noise than data collected during the final MT model measurements. If no filtering was employed the risk of showing false data, indicating non-significant differences in concentration, would have been high.

Both APS units used during this project underwent a simple functionality test during which standard polystyrene latex spheres were nebulized and detected. The particle sizes used were 0.9, 2, 3 and 5 μm. The APS units were overall good at classifying these particles correctly, however APS3 did not manage to distinguish particles < 2 μm. Due to this uncertainty, all DF data from APS3 below 2 μm was discarded in the final MT model measurements.

4 Results

4.1 Aerosol Generation

4.1.1 Fog Machine

The fog machine produced a fairly stable aerosol with a CMAD of 1.4 μm and GSD of 1.6. Generating a high enough concentration was not a problem, the APS limit for coincidence detection was easily exceeded. The high aerosol concentrations generated increased the humidity enough to cause condensation in the tubing, causing a possible threat to the APS during longer exposure times. For this reason, and because of previously reported problems for the APS instruments to provide accurate measurements on liquid droplets [Volckens and Peters, 2005], the fog machine aerosol was not used in any deposition measurements.

4.1.2 Dust Generator

The Palas dust generator produced a dry particle aerosol with a particle size distribution in the desired range. This particle generation method was used in all deposition measurements. An example of the particle size distribution generated using Spheriglass 5000 is seen in Figure 11. The distribution was measured at the inlet of the MT model with a 15 l/min flow through the standard, straight and no inclination angle, MT model. Data is plotted as raw

counts (black, left y-axis) and after transformation to normalised mass distribution (grey, right y-axis) for comparison (relevant for dose assessment in pharmaceutical applications). $dM/dlogD_p = dN/dlogD_p \cdot (\pi/6)D_p^3\rho$ for the mass distribution. From stability measurement data the average MMAD of the Spheriglass aerosol was found to be approximately 4.1/6.3 μm and the GSD 1.6/1.8 measured by APS2/APS3 respectively.

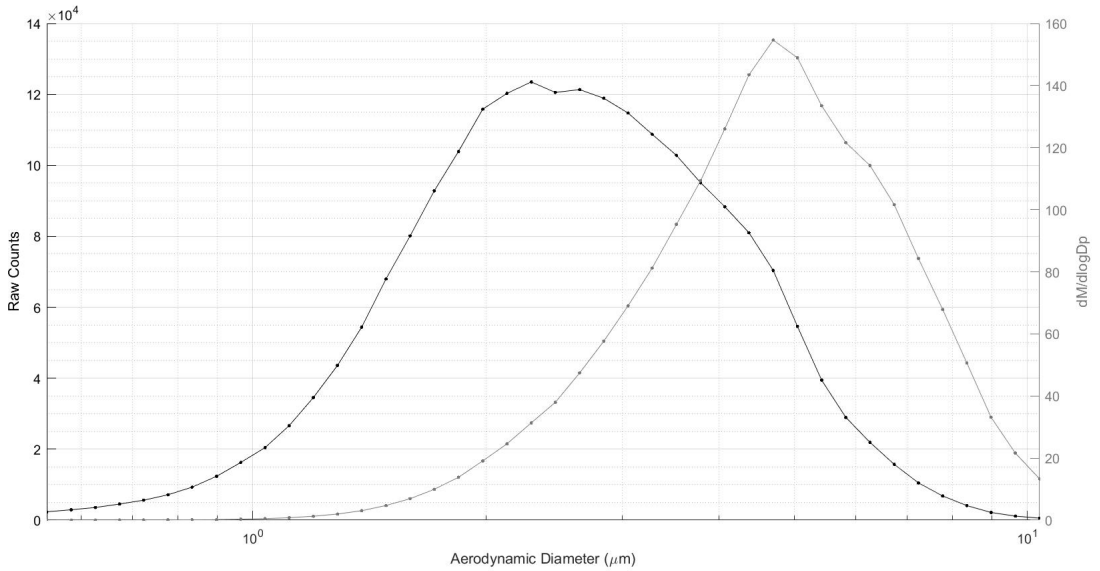

Figure 11: Particle size distribution measured by TSI APS 3321, generated by Palas BEG 1000 S using Spheriglass 5000. The distribution is plotted both as raw counts (black, left axis) and as a normalised mass-weighted distribution (grey, right axis) for comparison.

4.2 System Characterisation

All results from system characterisation are presented as unfiltered data, and will thus contain insignificant data points as a consequence of unstable aerosol generation, especially below 2 μm.

4.2.1 Stability Measurement

Figure 12 shows the data recorded during the stability measurement. Each marker represents one sample for a particular size channel. Each sample corresponds to a 30 s measurement, giving a total measurement time of more than three hours. During the measurement time the flow rate through the MT model was 30, 60 and 90 l/min, no difference is visible from alternating flow. This indicates that artefacts from non-isokinetic sampling are minimal at the model inlet sampling point. Each particle size seem fairly stable over long times. On the short time scale (a few minutes) the signal is quite noisy. Most particle sizes show a correlated variation. Aerosol generation is switched of around sample 350, resulting in a rapid decrease in particle concentration.

The particle size distribution during the stability measurement is plotted in Figure 13. Each line in the graph corresponds to a rolling average over five minutes, in total displaying

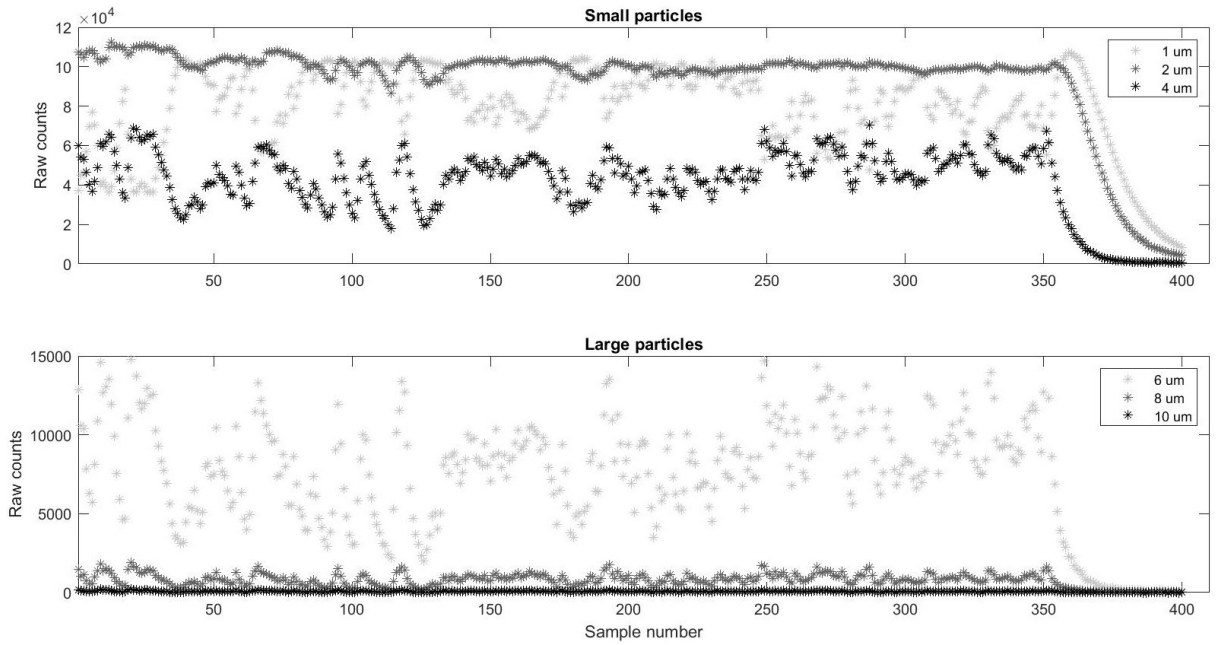

Figure 12: Aerosol generation stability during approximately three hours. Each marker corresponds to one sample of one APS particle size bin.

the particle size distribution during the entire active generation time. Size distributions measured early on in the series is plotted dark, and the distribution line gradually becomes lighter with time. The size distribution mode is centred around 1.5 μm (raw counts) as measured by both APS units. APS2 measured a log-normal distribution while APS3 indicated a heavy tail for large aerodynamic diameters.

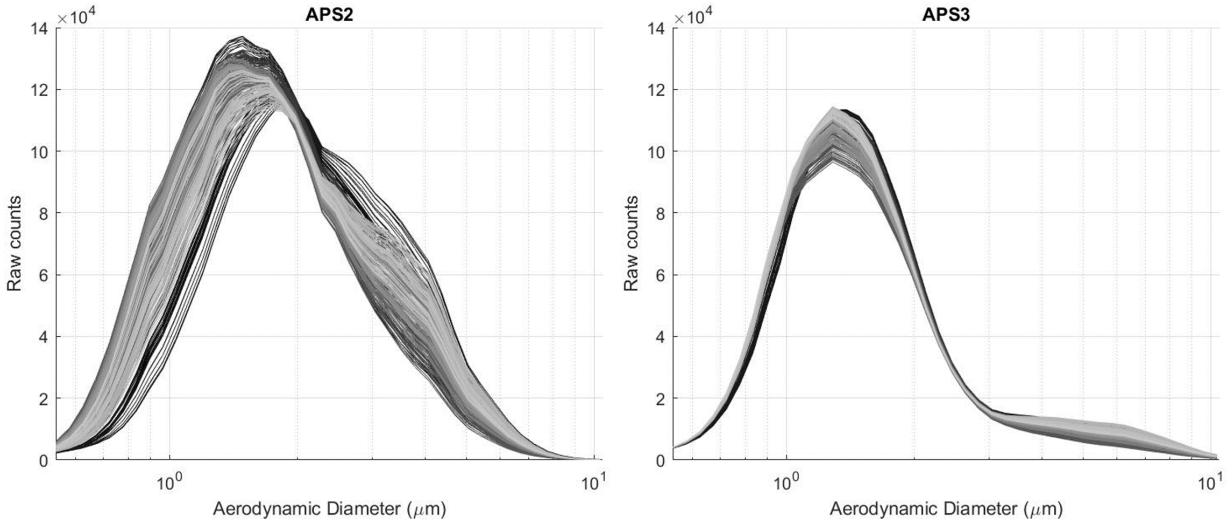

Figure 13: Particle size distribution (raw counts) plotted as a rolling average of five minutes during the three hour measurement time. The first average is plotted in black and each averaged line gradually gets lighter with time. Left: APS2, right: APS3.

APS2 measured a particle size distribution that shifts more during the measurement time. For particles with an aerodynamic diameter around 2 μm the concentration seem to decrease with time. For the other particle sizes there is no obvious trend, but size concentration fluctuates over time. APS3 showed less fluctuations in particle size distribution over time. The standard deviation of the averaged values in Figure 13 is plotted in Figure 14. This standard deviation data was used to filter the measured DF in the final MT model measurements as described in the methods section. From this data it looks as if APS2 have a maximum variation for particle diameters of approximately 1 and 3.5 μm. APS3 have an overall lower standard deviation with maximum centred around 1.5 and 6 μm. Both APS units have a minimum standard deviation in the interval 2-3 μm.

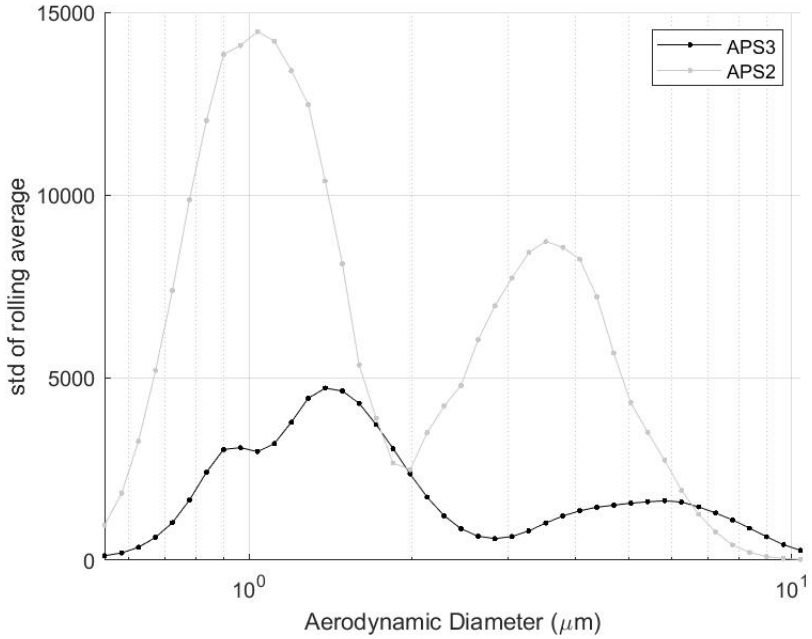

Figure 14: Standard deviation as a function of particle aerodynamic diameter for the rolling average in Figure 13.

From the stability measurement 100 observations (raw counts) from particles of small (2 μm), medium (4 μm) and large (8 μm) diameter were used to check normality of aerosol generation noise. The resulting normal probability plots are shown in Figure 15. Aerosol generation noise seems approximately normally distributed for most observations.

4.2.2 Coating Influence

The effect of silicone coating the standard model is demonstrated in Figure 16. The DF increases for larger particle sizes for both uncoated and silicone coated MT model, except for the largest particles in the uncoated 60 l/min measurement. For 60 and 90 l/min there is an increase in DF in the coated model for particles with diameters larger than 1.5 μm. For 15 l/min the same effect is seen above 4.5 μm. Negative deposition fractions below 2 μm are probably not significant given the low signal to noise ratio in this region.

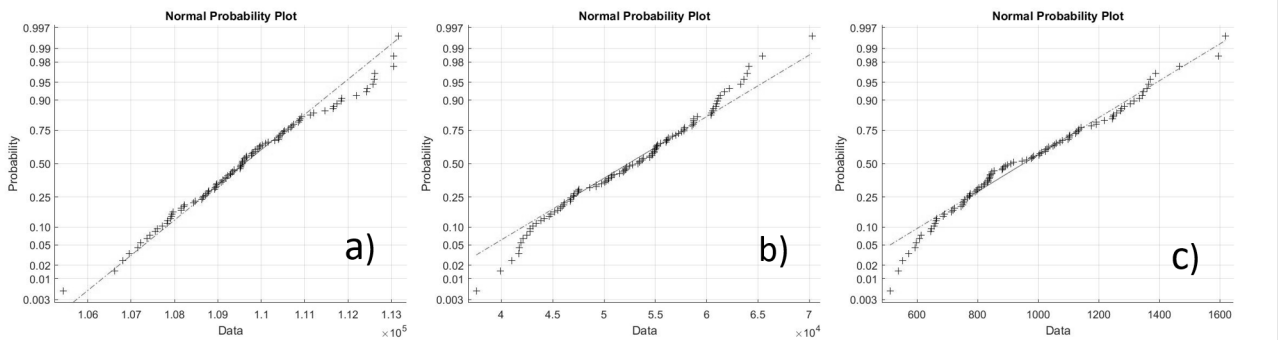

Figure 15: Normal probability plot of 100 observations during the stability measurement. The figure shows a) small, b) medium and c) large particles.

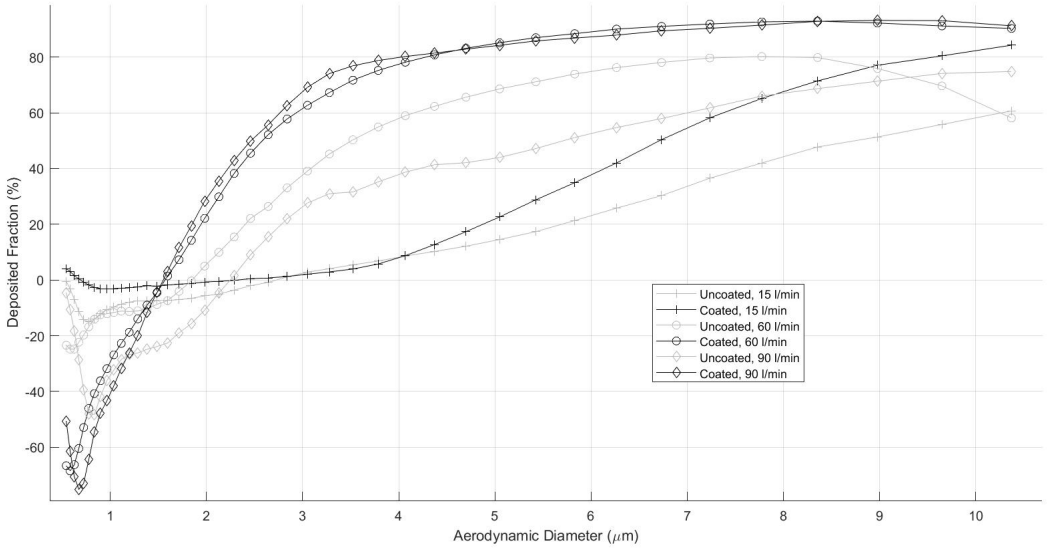

Figure 16: DF measured in the standard MT model without and with silicone coating for flows of 15, 60 and 90 l/min.

4.2.3 Repeatability Measurements

Figure 17 shows the average deposited fraction in the straight forward, no inclination model. This measurement was performed with 15, 60 and 90 l/min through the uncoated model, three times each. Data points representing the same flow measured on different days is almost overlapping in the interval between 2 and 8 μm. This shows that repeatability is high in this interval. At particle sizes above 8 μm the average DF deviates and repeatability seems lower. The data suggest that deposition is lowest for 15 l/min, a little higher for 90 l/min and the highest for 60 l/min. The overall trend is a decrease in recovered fraction for larger particle aerodynamic diameters. Negative deposition fractions below 2 μm are probably not significant given the low signal to noise ratio in this region, data here is also notably less consistent than for larger particle sizes.

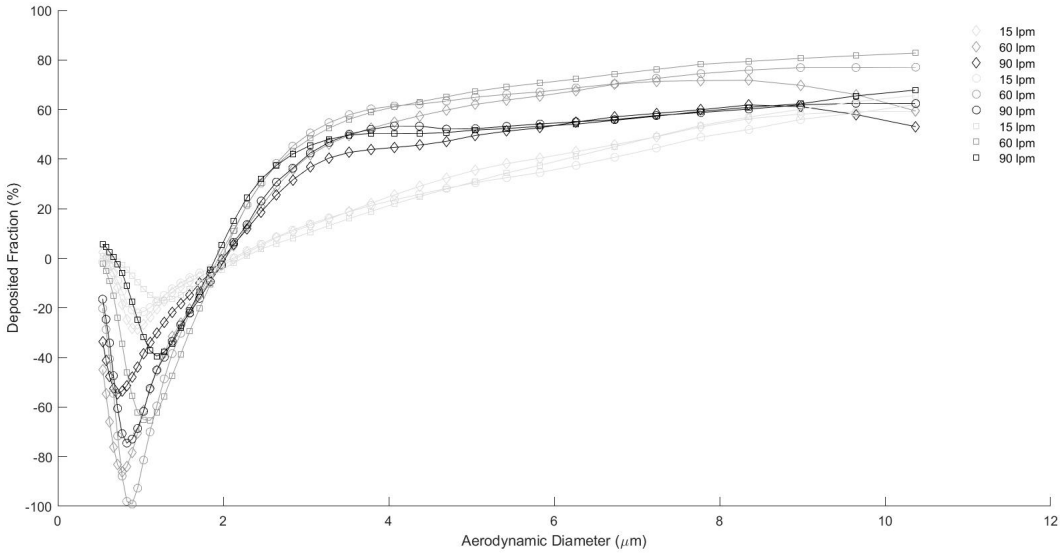

Figure 17: Repeatability measurement performed three times on straight forward, no inclination MT model. Repeated three times for 15, 60 and 90 l/min flow rates.

4.2.4 System Particle Loss

System particle loss, measured using an antistatic hose with an inner diameter of 25 mm bent to approximately 45 ° angle replacing the MT model, see Figure 9, is displayed in Figure 18. The values shown are mean values for all data collected by both APS units. Particle loss seem to increase with increasing particle diameter and flow rate for diameters $> 2\ \mu m$. Negative deposition fractions below 2 μm are probably not significant given the low signal to noise ratio in this region.

Figure 19 shows the DF measured in the isolated sampling tubes (including the 4-way valve). Data indicates increasing DF for particle diameters above 3 μm. High particle losses in the sampling tubes sets a limit to the sensitivity of the system, as a large amount of particles generated are not being detected. There is no apparent difference between the sampling tube used at the model inlet when compared to the outlet, i.e. the sampling tubes are symmetrical. This is important since the DF is calculated from the concentration at the outlet relative to the concentration at the inlet.

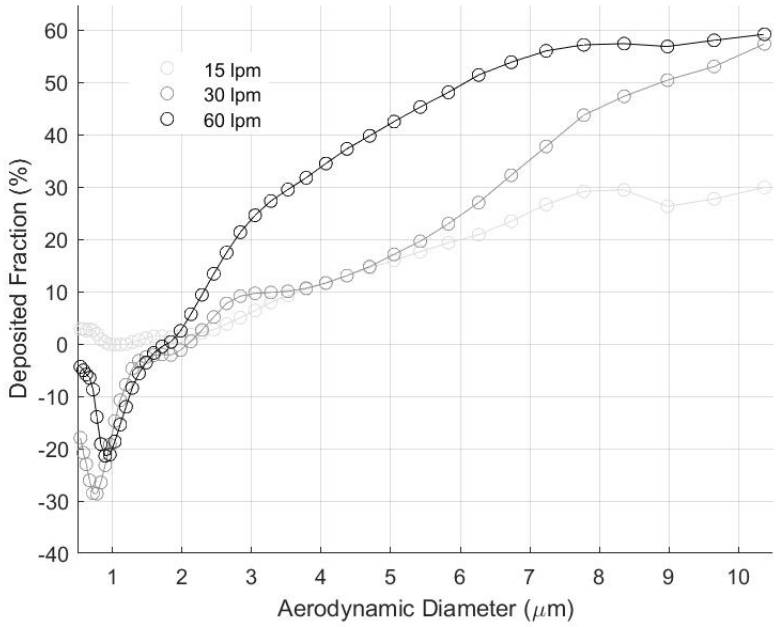

Figure 18: System particle loss measured using a hose replacing the MT model. Particle loss measured for flows of 15, 30 and 60 l/min.

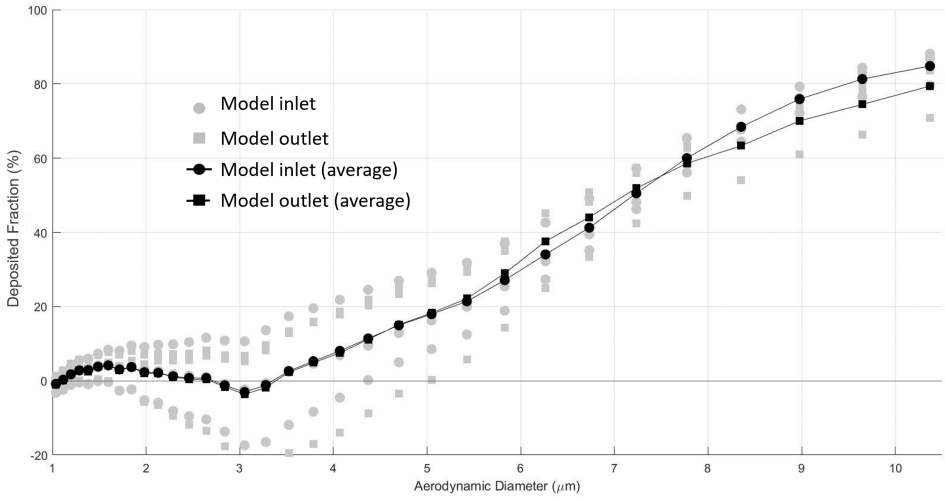

Figure 19: Estimated DF in sampling tubing, the tubing is connected to the model inlet and outlet respectively. This measurement did not include any MT model, only the sampling tubes and 4-way valve.

4.2.5 MT Model Data in General

As described in the methods section the sampling flow was switched five times during each MT model measurement series, resulting in collection of 30 minutes data before and after the MT models for each APS instrument. For large particle sizes this results in an alternating raw count signal as the one seen in Figure 20. Throughout all measurements in this project the low level in such a plot showed a low variation. However, the high level was not as stable over the measurement time and in some cases there was an apparent drift in the background (inlet sampling point) concentration. With this background the decision of averaging all three high levels and all three low levels, see b) in Figure 20, before calculating a DF in the final MT model measurements was made.

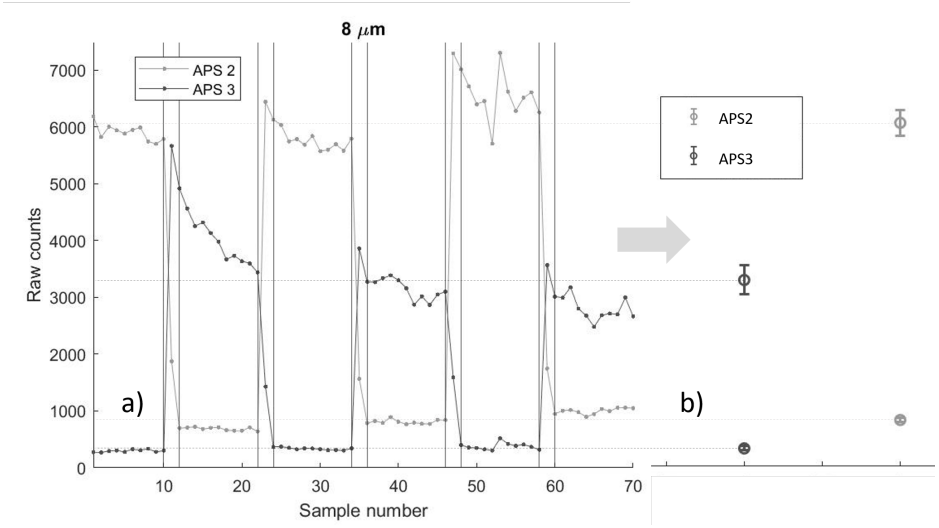

Figure 20: 8 μm particle raw counts during 70 samples, 30+5 minutes. The data in this plot was collected for the standard model at 60 l/min. a) Raw counts data. The alternation between high and low level corresponds to switching the valve controlling which APS unit is measuring at the inlet vs at the outlet of the MT model. b) Average and standard deviation for the three measured periods at the inlet and outlet respectively. Y-scale is the same as in a).

4.3 Final MT Model Measurements

All data throughout this section is filtered against the criteria that the difference between inlet and outlet is at least twice as large as the standard deviation, see section 3.5.1 for details. An overview of the DF data collected for MT models with 0, 15 and 30 ° inclination angle for flows of 15, 30 and 60 l/min is shown in Figure 21. No data points remained after filtering for a flow of 15 l/min through the 15 and 30 ° inlet inclination MT models. For the 0 ° inclination model a majority of the size bins have DF data from both APS units. Overall, more data points survived filtering for higher flows. The two APS units seem to correlate better for larger particle sizes than for smaller. For small particle diameters there is no clear trend which APS measures the highest DF. The one trend visible for all plots is increased DF for larger particles. For 0 ° 15 l/min, 30 ° 30 l/min and 30 ° 60 l/min APS3 indicates negative deposition for small particle sizes.

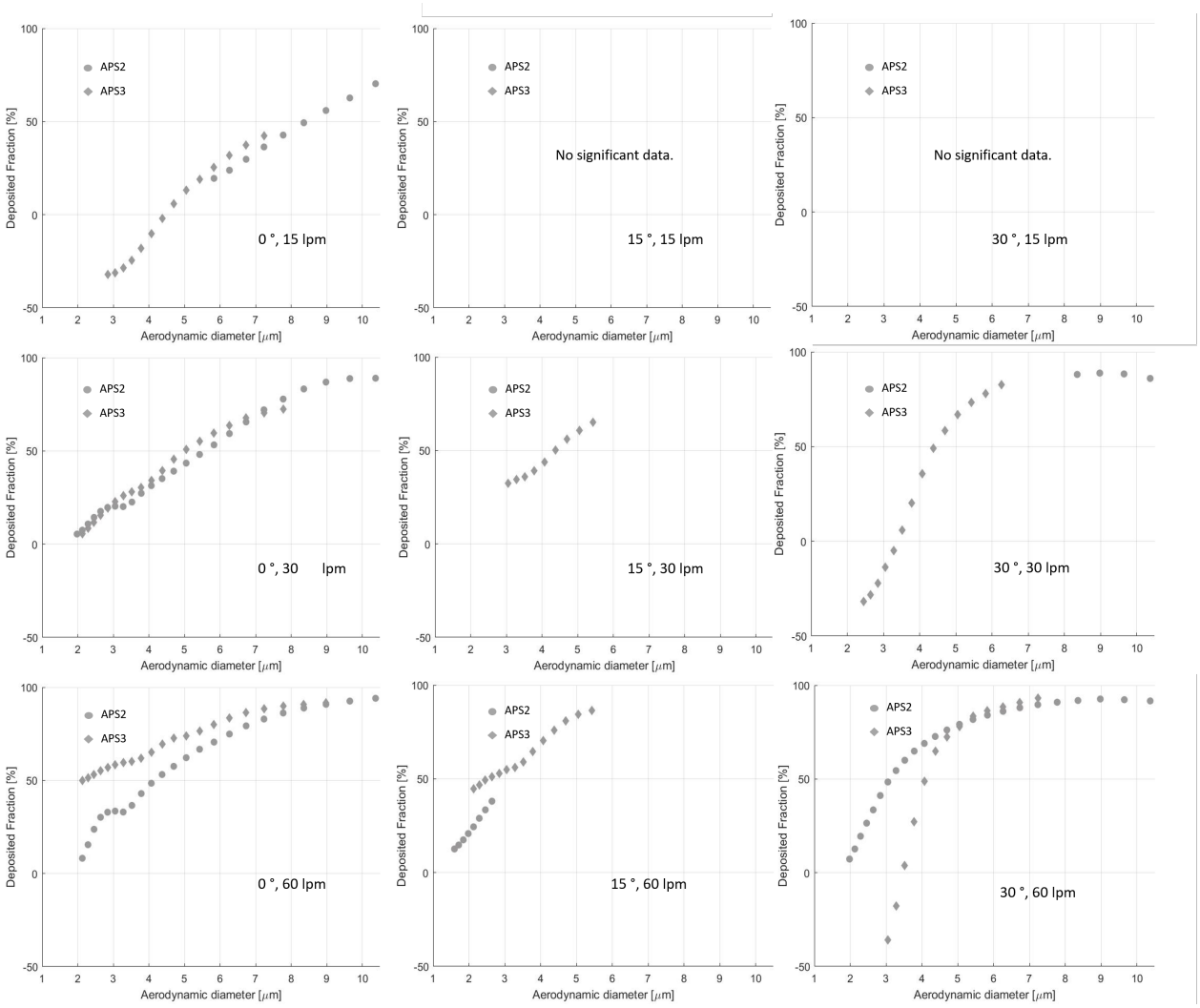

Figure 21: Overview of filtered DF from measurements on 0, 15 and 30 ° MT models at 15, 30 and 60 l/min. The different flow rates are shown as rows and inclination angles as columns. When available, data from both APS units is plotted.

The different inlet inclination angles (0, 15 and 30 °, 60 l/min) are compared to CFD modell values in Figure 22. Measured values are shown as dots, the average DF is plotted when data from both APS units remained after filtering. Modelled values are represented by asterisks connected by straight lines. The 0 ° measurement follows the line predicted by modelling reasonably well, but the modelled DF has a steeper curve. I.e. the measured DF is overestimated for small particles and underestimated for large particles when compared to modelling. For 15 ° the slope of the modelled curve coincides with the measured values, but measurements are shifted to the left in relation to the curve. No measured values are available at or above 6 μm. The measured data for 30 ° agrees well with the CFD model for most particle sizes. However, the DF is slightly underestimated for large diameters. The apparent jump in estimated DF at 3 μm is a result of averaging measurements, starting at that particle size bin (see also Figure 21).

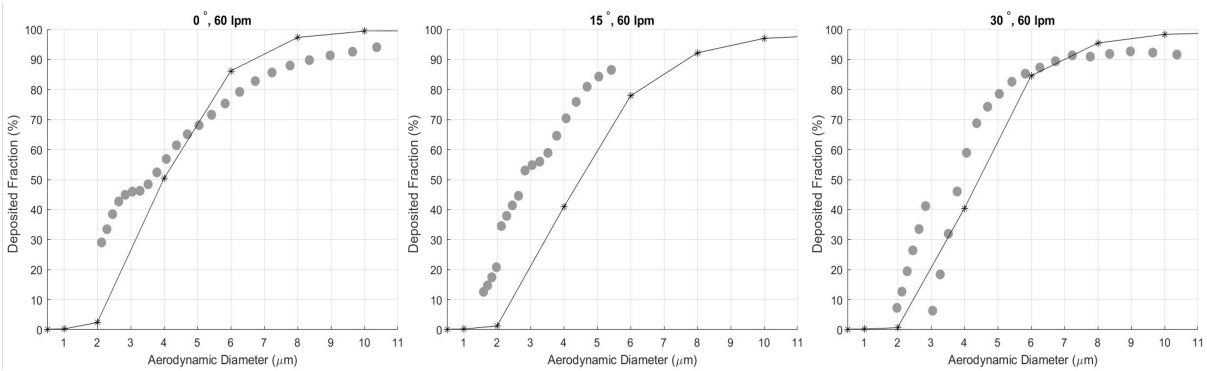

Figure 22: Comparison of filtered DF data (dotted line) and DF from CFD modelling (asterisks connected with lines) for 60 l/min flow. When more than one APS value is available the average DF is plotted. Left: 0 °, middle: 15 ° and right: 30 ° inlet inclination model.

Figure 23 contains the same data as the previous figure, but plotted in the same graph for comparison. The CFD model predicts small differences in DF for varying inclination angles. The highest DF for large particles was expected from 0 ° followed by 15 °, leaving 30 ° with the lowest DF. This trend is not visible for measured data.

The result of increasing flow rate (on 0 ° MT model only) compared to the DF values predicted by CFD modelling is shown in Figure 24. Measured values are shown as dots, the average DF is plotted when data from both APS units remained after filtering. Modelled values are represented by asterisks connected by straight lines. Data from 15 l/min measurement corresponds well to the CFD model for medium sized particles. No DF is available for smaller particle sizes and for large diameters the DF is underestimated, measured values do not show the sigmoid shape as predicted. 30 l/min also shows a straighter line for measured DF than expected from modelling, but the overall overlap is good. Small particle diameter DF is overestimated while large particle diameter (9.5 and 10.5 μm) DF is a little lower than expected. The same result is seen for 60 l/min, a higher DF for small particle sizes and a lower DF for larger diameters when comparing to modelled values.

Figure 25 contains the same data as the previous figure, but plotted in the same graph for comparison. Both the CFD model and measured values shows increasing DF for increasing flow rates.

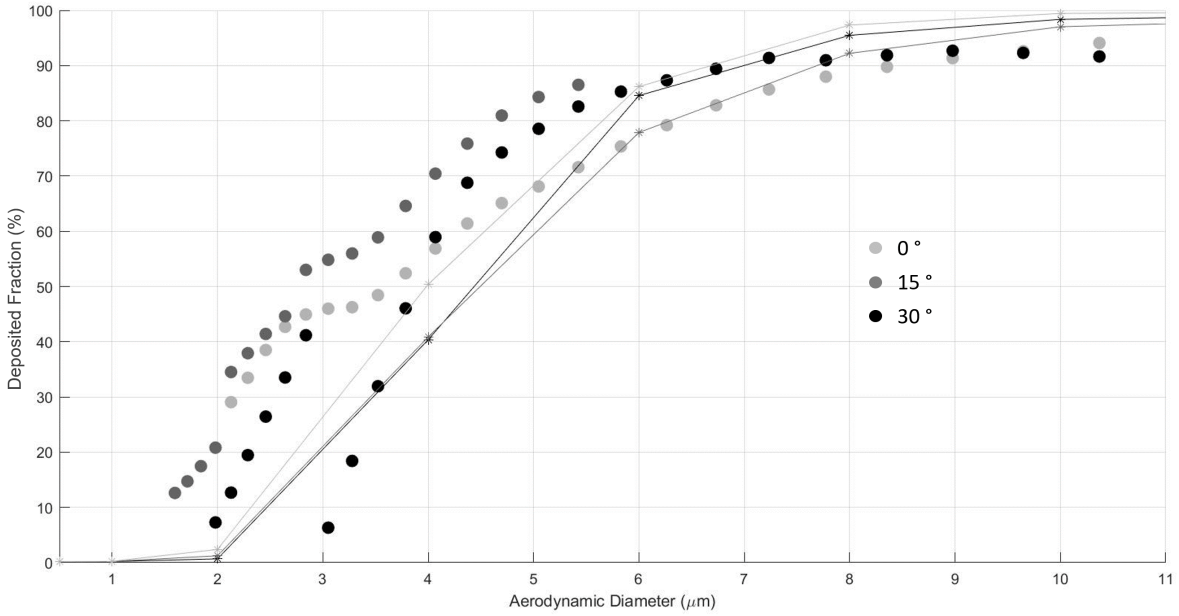

Figure 23: Comparison of filtered DF data (dotted lines) and DF from CFD modelling (asterisks connected with lines) for 60 l/min flow. When more than one APS value is available the average DF is plotted. 0 °, 15 ° and 30 ° inlet inclination model. All data plotted in the same graph for comparison of inclination angle effect.

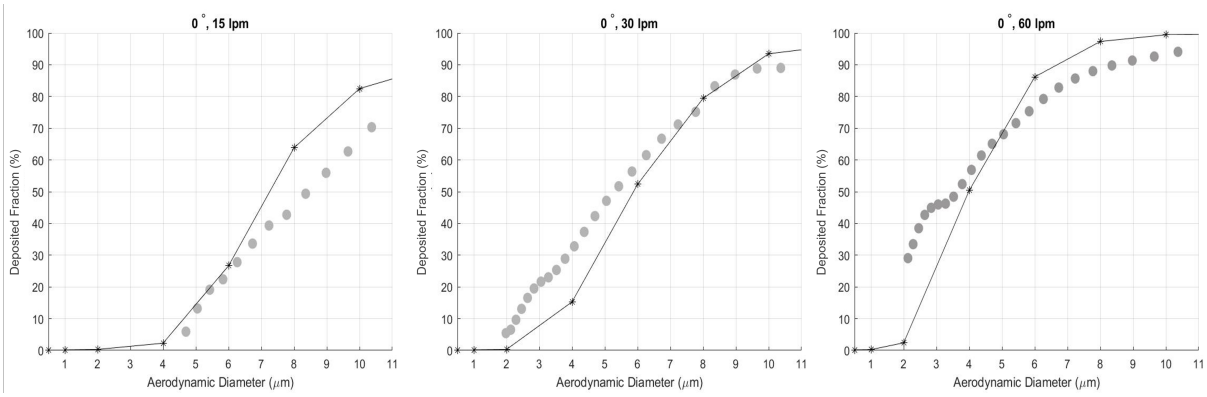

Figure 24: Comparison of filtered DF data (dotted line) and DF from CFD modelling (asterisks connected with lines) on 0 ° inclination MT model. When more than one APS value is available the average DF is plotted. Left: 15 l/min, middle: 30 l/min and right: 60 l/min.

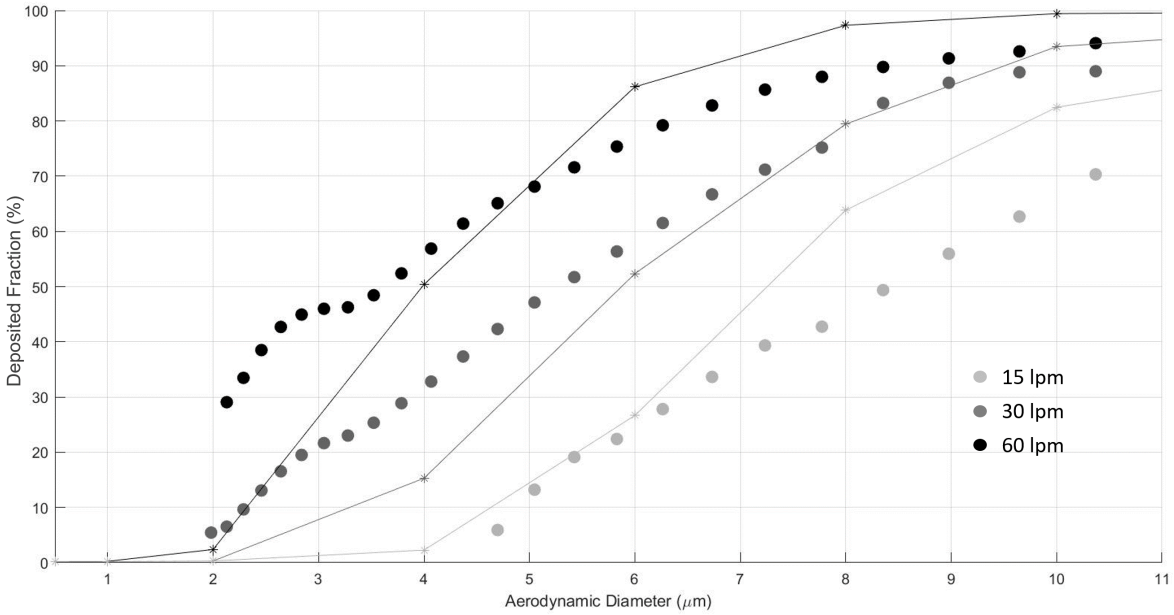

Figure 25: Comparison of filtered DF data (dotted line) and DF from CFD modelling (asterisks connected with lines) on 0 ° inclination MT model. When more than one APS value is available the average DF is plotted. The figure shows 15 l/min, 30 l/min and 60 l/min data. All data in the same graph for comparison.

5 Discussion

5.1 Aerosol Generation

Generating an aerosol with a fog machine was not a suitable option for this project since the aerosol size distribution had a CMAD of 1.4 μm, the fog machine did not create enough large particles. Condensation in the model, tubing and measurement instrument was also a major concern. The fog machine might have an advantage over the dry powder aerosol when it comes to the need of (re)coating models, but this was not investigated within this project. Another possible problem with using a liquid particle aerosol is, as presented in the background section, that counting efficiency is expected to decrease with particle size. However, the fog generator managed to produce a polydisperse aerosol in high concentrations, and may be useful for other applications thanks to its ease of operation.

The particle size distribution produced by the Palas generator was a reasonable fit to the project requirements of particles in the size range 1-10 μm. It was not ideal when measured as raw counts, particles of large diameter were relatively scarce. This resulted in a need to create a very high aerosol concentration to be able to get sufficient counting statistics for larger diameters. The mass-weighted particle size distribution looks more promising in that sense, but since the APS does not actually measure a mass weighted distribution but rather calculates it from scattering count data the high risk of large errors due to low counting statistics remains. The extreme concentrations needed because of this implies a risk of exceeding the coincidence limit in the detection volume, and missing counts as a consequence.

The glass dust, Spheriglass, should ideally have been dried previous to all measurements as this improved generation stability. By drying the powder agglomeration was reduced, allowing a more stable aerosol output from the Palas generator. However, the need of drying the powder was unfortunately discovered late in the project.

5.2 System Characterisation Measurements

As presented in Figure 12 the aerosol generated is not very stable over time. Looking at the part of the graph where the Palas generator is switched off there is a remarkably stable decrease in particle concentration for all sizes. This indicates that the problems with a noisy concentration is a direct effect of the generation method used, rather than the measurement setup. DF measurements are very sensitive to aerosol generation noise. Generation variations could be interpreted by mistake as deposition - if the background concentration drops at the same time as the sampling flow is switched from measuring at the model inlet to the model outlet it could result in false detection of a large DF. The risk of this type of error going unnoticed is partially reduced by using two APS units, allowing continuous monitoring at the model inlet. Data from both APS units could possibly be used in order to compensate for fluctuations in generated concentration. Within this project this problem have only been addressed by averaging the inlet and outlet levels over the whole measurement period, in an attempt to smooth out possible variations in the aerosol concentration evenly. The aerosol generation noise could possibly be reduced physically as well, still using the same generator, by increasing the mixing volume and thus smoothing out the generated concentration in time. The aerosol generation stability was a major concern, and the reason why filtering of data was necessary before presentation of final MT model deposition results.

The variation in particle size distribution, Figure 13 and 14, is a cause for concern. First of all the two APS units should measure the same distribution when sampling from the same volume simultaneously. When measured manually using a flow meter the aerosol flow in the APS was also found to differ significantly between the two units. APS2 had an aerosol flow of approximately 1.0 l/min and APS3 1.5 l/min. The specified values for this parameter for APS model 3321 is 1 l/min, which is also the value indicated by both instruments internal measurements. Practically this means that APS3 have a higher flow than it is calibrated against, particles travel faster through the detection volume than intended, reducing the TOF, and are miss-classified as smaller than they really are. Looking at the measured particle size distribution for APS3 we would then expect it to be shifted towards smaller particles compared to the distribution of APS2, but this is not the case. All together this indicates that at least one of the two is wrong in its size classification and requires calibration and/or service.

The two instruments also showed large differences in variation during the measurement time. APS2, detecting a much higher variation and also total count rate, could be more sensitive than APS3 and therefor able to distinguish any drifts in aerosol concentration. The minimum in standard deviation for both APS units around 2 μm could be an effect of particle sizes used for calibration, making the instruments better at classifying this size. One possibility to reduce the effect of any drift on the calculated DF is to group APS size bins together, although this would also reduce the size resolution.

The coating measurements demonstrated that coating the inside of the MT model had

a large effect on the DF. The model was not recoated between measuring the different flows, this could be a possible explanation to why the DF did not increase when going from 60 l/min to 90 l/min for the coated model whereas it did so for the uncoated. The coating could have been saturated with aerosol, causing some particles to bounce off the surface instead of sticking during the last measurement (90 l/min). This theory is the reason why all models were recoated for each flow in the final MT model measurements. For small particles and high flows DF seem negative in the coating measurement. This could perhaps be a consequence of deposited particles not sticking properly to the coating. Also, this plot displays a calculated DF even if the difference between model inlet and outlet is indistinguishable from the generation noise, which is particularly problematic for particles with diameters below 2 μm where the variation in generation is at its highest.

The repeatability of the measurements, Figure 17, was generally very good. Repeatability would probably be even higher if the measurement had been performed with a more stable aerosol generation. The result that DF was highest for 60 l/min, rather than 90 l/min, was surprising since impaction increases with flow rate. A possible explanation to this is that the model was not recoated between each flow rate measurement, only at the end of each measurement day. That repeatability seem lower for large particles could be explained by low counting statistics.

System particle loss was tricky to estimate. The measurements on DF in the antistatic hose give an indication on what happens in a simple geometry. The estimated DF in the hose was lower than that found in the final MT model measurements, indicating at least some degree of sensitivity in the system. The flow constriction needed to attach the hose to the funnel in the horizontal ventilation tube, see Figure 9, probably had a large effect on the DF. Deposition increased with increasing flow rate, as expected from increasing inertial impaction and turbulence. Results from measuring DF in the sampling tubes, comparing inlet and outlet tube, supported the design idea that as long as the bends were smooth, and essentially the only difference between inlet and outlet sampling tube was a vertical distance, this would no distort sampling. The DF measured both for the inlet and outlet sampling tube was disturbingly high, and is probably part of the problem in getting sufficient counting statistics for large particle diameters. Also the fact that the sampling tubes are angled 45 $^{\circ}$ in relation to the flow direction gives a decreased aspiration efficiency and thus lower counts, particularly for large particles. For the final DF this should have no major effect since it was a relative measurement and sampling was performed symmetrically at the inlet and outlet.

Throughout this project it has been assumed that no losses occur between the two sampling points except for inside the MT model. However, this is probably not the case in reality. The problem is somewhat reduced by not coating these surfaces, making less particles stick to them. This assumption could affect our measurements to over-estimate the DF in the MT model. The size of this error is hard to estimate, but it should be relatively small in relation to the deposition studied, as the MT model have a much smaller diameter and more complex geometry. It was also noted that the amount of particles in the funnel and around the sampling tube after a measurement was considerably less than in the MT models. Another note on this is the assumption that, even though sampling is not performed isokinetically, the sampling conditions are similar between the two sampling points. The result in Figure 12, where no effect from changing flow rates is seen, indicates that effects from anisokinetic sampling are small. It is hard to know what the flow pattern looks like at the inlet and outlet

sampling point, considering that the aerosol flows through a funnel that is oriented in the opposite direction for the outlet when compared to the inlet. However, the volume where the sample is collected is the same and the flow is laminar, and as the same flow that enters the inlet funnel also enters the exit funnel there should be little difference in the linear gas velocity between inlet and outlet sampling point. Since the linear flow velocity is higher in the APS sampling tube than in the funnel, Table 1, large particles could be underestimated due to their higher inertia and inability to follow the air stream into the sampling tube. However, this effect is expected to be similar at both the inlet and outlet sampling point. To avoid distortion of the particle size distribution due to sampling aspiration the sampling tube should optimally be switched for each flow. I.e. the APS sampling tube should have the largest diameter for the flow rate of 15 l/min and the smallest for 60 l/min. This of course poses new problems in the system design, such as losses when the sampling tube is connected to the fixed diameter inlet of the APS.

5.3 Final MT Model Measurements

The filtering of the final MT model data removed a lot of data points, particularly for 15 l/min. The DF is expected to be lower for a lower flow, possibly explaining why the difference between the high and low level did not meet the filtering criteria. Most data points remained for 0 ° model, this was probably an effect of powder being dried only during this experiment and through this aerosol generation became more stable. All data indicated increased DF for larger particle diameters, as expected from increased inertial impaction. For smaller particle diameters the two APS unit measurements differed more. This could be related to that the filtering criteria, std in Figure 14, have a minimum for both APS units in the interval 2-3 μm. APS3 still indicated negative DF for small diameters in the measurement on 0 ° 15 l/min, 30 ° 30 l/min and 30 ° 60 l/min. This would mean that more particles exits the model than the amount entering. Considering that all models were coated and thus should not loose any deposited particles, and particles can not be created inside the model, this is not probable. Looking closer at the raw counts for those size bins, see example from 30 ° 60 l/min in Figure 28, the particle concentration seem very unstable during these particular measurements in APS3. This leads to distorted averages and strange effects in the DF. The concentration of small particles measured by APS3 were lower than for APS2, making the change in concentration more detrimental. Extending the outlet sampling tube for 15 and 30 ° was necessary to connect the models, but could have affected the measurement. If it had an effect we would expect to measure a higher DF due to particle loss in the extra tubing. Since the extra tubing was short, straight and close to vertical any errors from this is expected to be small and should have no major effect compared to the CFD model results.

The results in Figure 22 and 24 shows that measured data is close to the DF caluclated by the CFD model. The lowest deposition is seen for low flows, in line with the recommendation that aerosols for therapeutic use should have a flow rate of less than 30 l/min to reduce the risk of deposition due to turbulence in the trachea [Darquenne, 2012] and increased inertial impaction. The CFD model fit would probably be even better if the aerosol generation fluctuated less. Also more sensitive filtering criteria would probably help in determining the most relevant measurement points. Optimally the filtering should be able to tell not only when there is a sufficient difference in inlet and outlet concentration, but also

be sensitive to short-term variations in concentration distorting the DF value. Perhaps it would be possible to filter out values when only one APS show tendencies of large concentration variation. Taking this one step further one APS could be used to monitor the inlet concentration the whole measurement time, giving a reference signal to compare with the APS measuring the DF. Even though this could possibly be a solution to handling drifts in aerosol generation, a more complex measurement system would come with the disadvantage of potentially introducing more uncertainty in data.

The overall most important detail to improve was the aerosol generation stability. By getting less noise in the inlet signal, filtering would remove less data and sensitivity would be improved. Even small improvements on the stability, such as drying the particles, seemed to be important for the data quality of the final MT measurements.

5.4 Conclusions

During this project a method for measuring deposition of particles in the size range 1-10 μm in a MT model has been developed. The method was evaluated, both with and without the presence of the standard MT model for several flow rates ranging from 15 to 90 l/min. Deposition was measured for MT models with three different inlet angles at flows of 15, 30 and 60 l/min. MT models representing subject head orientation were excluded from the project.

The measured (and filtered) DF in MT models was qualitatively similar to data estimated by the CFD model. For the standard MT model both modelled and measured values indicated a higher DF for a higher flow rate. Data also consistently showed higher deposition for larger particle diameters. It was not possible to distinguish any difference between the different models representing aerosol inlet plume angle, but such a relationship could neither be disproved.

The intervariation between the two APS units used was larger than expected. No conclusions on which APS were the better choice could be drawn, and an average was used to show the resulting DF after filtering data for final MT measurements. Aerosol generation stability was found to be key to generating higher quality data. Related to this is drying the powder before use to reduce agglomeration. Coating had a large effect on the deposition, and regular recoating seem necessary to ensure that deposited particles stick to the surface.

Apart from improving the generation stability it would be beneficial to find more efficient filtering criteria. Hopefully this could also reduce any remaining problems with varying concentration. Reliable measurement instruments, the two APS units in this case, is also a prerequisite to collect valid deposition data. Assuming these technical challenges could be solved, the method developed has high potential of delivering high quality deposition data on MT models.

References

[Baron et al., 2011] Baron, P. A., Kulkarni, P., and Willeke, K. (2011). *Aerosol Measurement - Principles, Techniques, and Applications*. Wiley, third edition.

[Borgström et al., 2006] Borgström, L., Olsson, B., and Thorsson, L. (2006). Degree of throat deposition can explain the variability in lung deposition of inhaled drugs. *Journal of Aerosol Medicine: Deposition, Clearance, and Effects in the Lung*, 19(4):473–483.

[Brown, 2015] Brown, J. S. (2015). Deposition of Particles. In *Comparative Biology of the Normal Lung*, chapter 27, pages 513–536. Elsevier, London, 2 edition.

[Burnell et al., 2007] Burnell, P. K. P., Asking, L., Borgström, L., Nichols, S. C., Olsson, B. O., Prime, D., and Shrubb, I. (2007). Studies of the Human Oropharyngeal Airspaces Using Magnetic Resonance Imaging IV-The Oropharyngeal Retention Effect for Four Inhalation Delivery Systems. *JOURNAL OF AEROSOL MEDICINE*, 20(3).

[Byron et al., 2010] Byron, P. R., Hindle, M., Lange, C. F., Longest, P. W., McRobbie, D., Oldham, M. J., Olsson, B., Thiel, C. G., Wachtel, H., and Finlay, W. H. (2010). In vivo-in vitro correlations: Predicting pulmonary drug deposition from pharmaceutical aerosols. *Journal of Aerosol Medicine and Pulmonary Drug Delivery*, 23(SUPPL. 2).

[Darquenne, 2012] Darquenne, C. (2012). Aerosol Deposition in Health and Disease. *Journal of Aerosol Medicine and Pulmonary Drug Delivery*, 25(3):140–147.

[Darquenne and Prisk, 2004] Darquenne, C. and Prisk, G. K. (2004). Aerosol deposition in the human respiratory tract breathing air and 80:20 heliox. *Journal of Aerosol Medicine: Deposition, Clearance, and Effects in the Lung*, 17(3):278–285.

[DeHaan and Finlay, 2001] DeHaan, W. H. and Finlay, W. H. (2001). In vitro monodisperse aerosol deposition in a mouth and throat with six different inhalation devices. *Journal of Aerosol Medicine: Deposition, Clearance, and Effects in the Lung*, 14(3):361–367.

[Delvadia et al., 2012] Delvadia, R. R., Longest, P. W., and Byron, P. R. (2012). In vitro tests for aerosol deposition. i: Scaling a physical model of the upper airways to predict drug deposition variation in normal humans. *Journal of Aerosol Medicine and Pulmonary Drug Delivery*, 25(1):32–40.

[Fadl et al., 2007] Fadl, A., Wang, J., Zhang, Z., and Sung Cheng, Y. (2007). Effects of MDI spray angle on aerosol penetration efficiency through an oral airway cast. *Journal of Aerosol Science*, 38(8):853–864.

[Golshahi et al., 2013] Golshahi, L., Noga, M. L., Vehring, R., and Finlay, W. H. (2013). An in vitro study on the deposition of micrometer-sized particles in the extrathoracic airways of adults during tidal oral breathing. *Annals of Biomedical Engineering*, 41(5):979–989.

[Grgic et al., 2004] Grgic, B., Finlay, W. H., and Heenan, A. F. (2004). Regional aerosol deposition and flow measurements in an idealized mouth and throat. *Journal of Aerosol Science*, 35(1):21–32.

[Heenan et al., 2004] Heenan, A. F., Finlay, W. H., Grgic, B., Pollard, A., and Burnell, P. K. (2004). An investigation of the relationship between the flow field and regional deposition in realistic extra-thoracic airways. *Journal of Aerosol Science*, 35(8):1013–1023.

[Heyder, 1975] Heyder, J. (1975). Gravitational deposition of aerosol particles within a system of randomly oriented tubes. *Journal of Aerosol Science*, 6(2):133–137.

[Heyder et al., 1986] Heyder, J., Gebhart, J., Rudolf, G., Schiller, C. F., and Stahlhofen, W. (1986). Deposition of particles in the human respiratory tract in the size range 0.005-15 μm. *Journal of Aerosol Science*, 17(5):811–825.

[Hinds, 1999] Hinds, W. C. (1999). *Aerosol Technology*. John Wiley & Sons, Inc, second edition.

[Huang et al., 2020] Huang, F., Zhu, Q., Zhou, X., Gou, D., Yu, J., Li, R., Tong, Z., and Yang, R. (2020). Role of CFD based in silico modelling in establishing an in vitro-in vivo correlation of aerosol deposition in the respiratory tract. *Advanced Drug Delivery Reviews*.

[ICRP, 1994] ICRP (1994). Human respiratory tract model for radiological protection. Technical Report ICRP Publication 66, International Commission on Radiological Protection. *ICRP Publication 66. Ann. ICRP*, 24.

[Labiris and Dolovich, 2003] Labiris, N. R. and Dolovich, M. B. (2003). Pulmonary drug delivery. Part I: Physiological factors affecting therapeutic effectiveness of aerosolized medications. *British Journal of Clinical Pharmacology*, 56(6):588–599.

[Löndahl et al., 2014] Löndahl, J., Möller, W., Pagels, J. H., Kreyling, W. G., Swietlicki, E., and Schmid, O. (2014). Measurement techniques for respiratory tract deposition of airborne nanoparticles: A critical review.

[Longest et al., 2009] Longest, P. W., Hindle, M., and Das Choudhuri, S. (2009). Effects of Generation Time on Spray Aerosol Transport and Deposition in Models of the Mouth-Throat Geometry. *JOURNAL OF AEROSOL MEDICINE AND PULMONARY DRUG DELIVERY*, 22(2):67–83.

[Melandri et al., 1983] Melandri, C., Tarroni, G., Prodi, V., De Zaiacomo, T., Formignani, M., and Lombardi, C. C. (1983). Deposition of charged particles in the human airways. *Journal of Aerosol Science*, 14(5):657–669.

[Peters and Leith, 2003] Peters, T. M. and Leith, D. (2003). Concentration measurement and counting efficiency of the aerodynamic particle sizer 3321. *Journal of Aerosol Science*, 34(5):627–634.

[Pfeifer et al., 2016] Pfeifer, S., Müller, T., Weinhold, K., Zikova, N., Martins, S., Santos, D., Marinoni, A., Bischof, O. F., Kykal, C., Ries, L., Meinhardt, F., Aalto, P., Mihalopoulos, N., and Wiedensohler, A. (2016). Intercomparison of 15 aerodynamic particle size spectrometers (APS 3321): uncertainties in particle sizing and number size distribution. *Atmos. Meas. Tech*, 9:1545–1551.

[Stylianou et al., 2017] Stylianou, F. S., Angeli, S. I., Kassinos, S. C., and Svensson, M. (2017). The Effect of Flow Rate, Head Position, and Inhaler Orientation on the Air Flow and Particle Deposition in an MRI-Based Mouth-Throat Geometry. In *10th International Symposium on Turbulence and Shear Flow Phenomena*, Chicago.

[Taulbee and Yu, 1975] Taulbee, D. B. and Yu, C. P. (1975). A theory of aerosol deposition in the human respiratory tract. *Journal of Applied Physiology*, 38(1):77–85.

[TSI, 2012] TSI (2012). Aerodynamic Particle Sizer Model 3321 - Theory of Operation.

[Volckens and Peters, 2005] Volckens, J. and Peters, T. M. (2005). Counting and particle transmission efficiency of the aerodynamic particle sizer. *Journal of Aerosol Science*, 36(12):1400–1408.

[Wang et al., 2016] Wang, H., Naghavi, M., Allen, C., Barber, R. M., Carter, A., Casey, D. C., Charlson, F. J., Chen, A. Z., Coates, M. M., Coggeshall, M., Dandona, L., Dicker, D. J., Erskine, H. E., Haagsma, J. A., Fitzmaurice, C., Foreman, K., Forouzanfar, M. H., Fraser, M. S., Fullman, N., ..., and Zuhlke, L. J. (2016). Global, regional, and national life expectancy, all-cause mortality, and cause-specific mortality for 249 causes of death, 1980–2015: a systematic analysis for the Global Burden of Disease Study 2015. *The Lancet*, 388(10053):1459–1544.

[Welker, 2012] Welker, R. W. (2012). Basics and Sampling of Particles for Size Analysis and Identification. In *Developments in Surface Contamination and Cleaning: Detection, Characterization, and Analysis of Contaminants*, pages 1–80. Elsevier Inc.

[Widmaier et al., 2014] Widmaier, E., Raff, H., and Strang, K. (2014). Respiratory Physiology. In *Vander's Human Physiology: The Mechanisms of Body Function*, chapter 13, pages 446–473. McGraw-Hill, New York, 13th edition.

[Worth Longest and Hindle, 2009] Worth Longest, P. and Hindle, M. (2009). Evaluation of the respimat soft mist inhaler using a concurrent cfd and in vitro approach. *Journal of Aerosol Medicine and Pulmonary Drug Delivery*, 22(2):99–112.

Appendix A - Supplementary Information

Stability Measurement

Figure 26 shows the MMAD and GSD over time, as found during the stability measurement. Figure 27 compares raw counts as measured by APS2 and APS3. The plotted data was collected during the stability measurement and the figure shows 70 samples, corresponding to the measurement time of 30+5 minutes. The figure indicates that there is a difference in the particle size distribution as measured by the two APS units. For 6 μm particles the APS units correlates well. Looking at 1, 2 and 4 μm data APS2 seem to show a larger spread in detected raw counts. The overall relationship between the two units seem linear for each particle size bin.

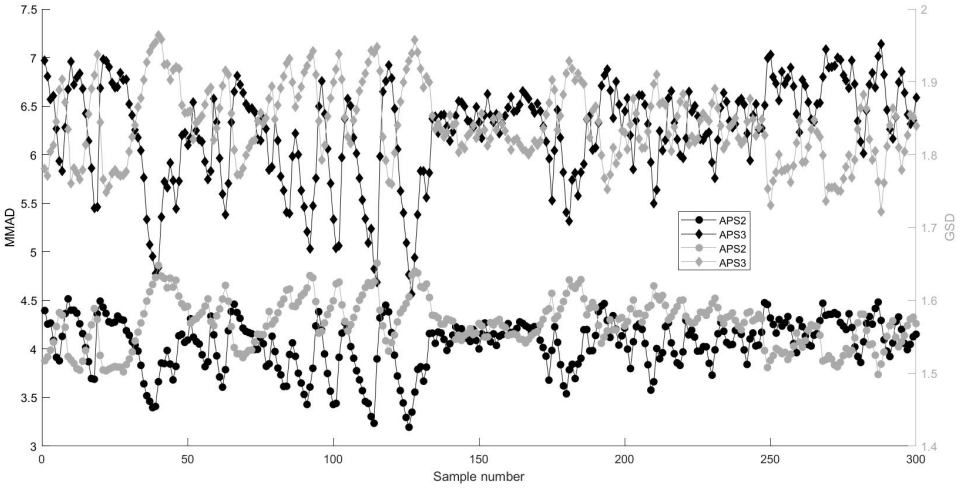

Figure 26: MMAD and GSD over three hour measurement time for both APS units measuring the same volume. Left y-axis MMAD and right y-axis GSD.

Final MT Model Measurements

Figure 28 shows variation in raw counts for small particles caused by a fluctuating aerosol generation. Data was collected from the 0 ° MT model for 60 l/min.

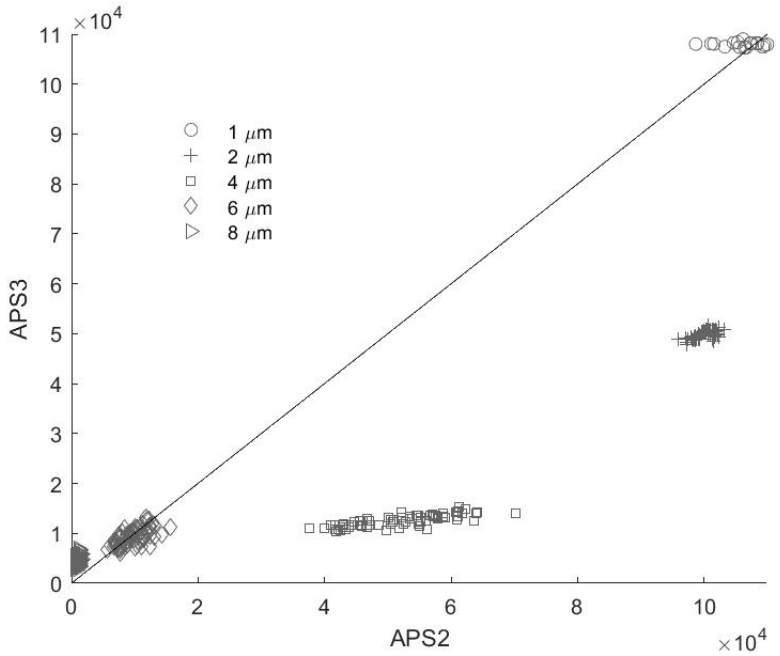

Figure 27: Comparison of APS2 and APS3 measuring the same volume simultaneously. Raw count data from APS2 is plotted against raw counts as measured by APS3.

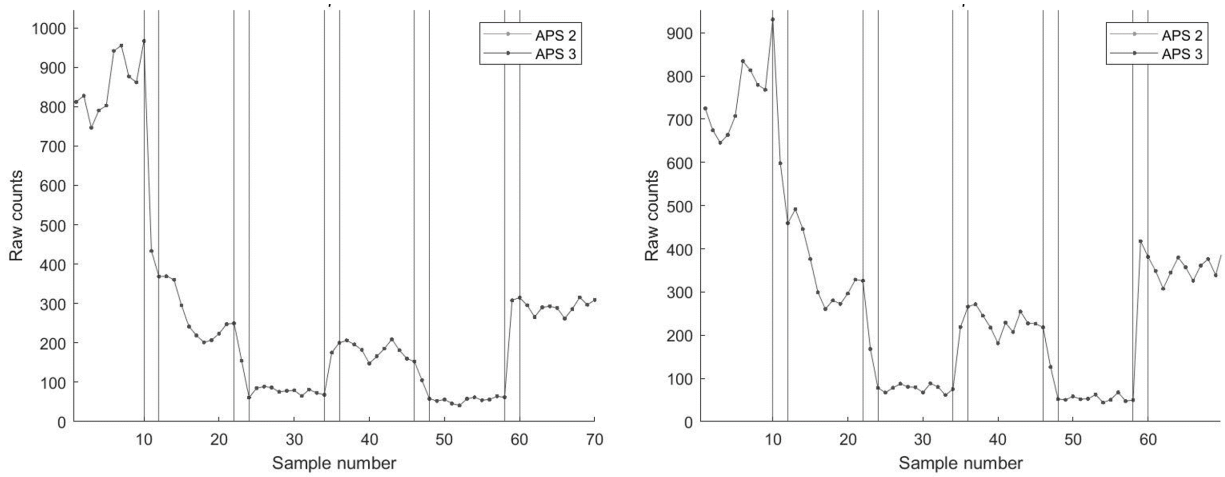

Figure 28: Raw counts measured by APS3 for 30 ° MT model at 60 l/min. Left: 3 μm particles. Right: 3.5 μm particles.

Appendix B - Final MT Model Measurement Data

Unfiltered raw count data for all measurements presented in Figure 21 is given in Table 7.1-3.

Table 2: Unfiltered deposited fraction for final MT model measurements. DF x, y, z denotes inhaler inlet angle (which MT model), flow rate in l/min, APS ID. Particle sizes 0.5 to 1.7 μm.

Diameter (μm)	0.542	0.583	0.626	0.673	0.723	0.777	0.835	0.898	0.965	1.037	1.114	1.197	1.286	1.382	1.486	1.596	1.715
DF 0, 15, 2	0.10	0.09	0.09	0.09	0.09	0.09	0.08	0.07	0.06	0.04	0.01	-0.01	-0.05	-0.08	-0.12	-0.12	-0.11
DF 0, 15, 3	-0.13	-0.13	-0.14	-0.13	-0.14	-0.13	-0.14	-0.14	-0.14	-0.14	-0.14	-0.15	-0.15	-0.16	-0.17	-0.17	-0.19
DF 0, 30, 2	0.27	0.25	0.21	0.14	-0.01	-0.29	-0.71	-1.12	-1.16	-0.88	-0.64	-0.47	-0.35	-0.23	-0.12	-0.06	-0.01
DF 0, 30, 3	0.04	0.03	0.03	0.02	0.02	0.02	0.01	0.01	0.01	0.00	0.00	0.00	0.00	0.00	0.01	0.01	0.01
DF 0, 60, 2	0.45	0.44	0.42	0.39	0.34	0.23	0.00	-0.54	-1.47	-2.31	-2.51	-2.24	-1.69	-1.05	-0.56	-0.32	-0.17
DF 0, 60, 3	0.48	0.48	0.47	0.46	0.46	0.46	0.46	0.45	0.45	0.45	0.45	0.46	0.46	0.47	0.47	0.48	0.48
DF 15, 15, 2	0.08	0.09	0.10	0.10	0.09	0.09	0.09	0.08	0.07	0.06	0.05	0.04	0.02	0.01	0.00	-0.01	-0.01
DF 15, 15, 3	0.26	0.27	0.27	0.26	0.25	0.25	0.25	0.25	0.26	0.25	0.25	0.25	0.25	0.25	0.26	0.26	0.26
DF 15, 30, 2	-0.10	-0.09	-0.08	-0.07	-0.06	-0.05	-0.04	-0.04	-0.04	-0.03	-0.03	-0.03	-0.03	-0.03	-0.03	-0.03	-0.03
DF 15, 30, 3	0.27	0.24	0.24	0.28	0.27	0.27	0.27	0.26	0.26	0.28	0.28	0.28	0.27	0.27	0.28	0.26	0.26
DF 15, 60, 2	0.02	0.02	0.02	0.03	0.03	0.04	0.05	0.06	0.06	0.07	0.07	0.08	0.09	0.10	0.11	0.13	0.15
DF 15, 60, 3	0.49	0.49	0.48	0.46	0.45	0.45	0.46	0.47	0.47	0.47	0.47	0.46	0.48	0.46	0.45	0.44	0.43
DF 30, 15, 2	0.12	0.13	0.13	0.12	0.09	0.06	0.04	0.03	0.02	0.01	0.01	0.00	-0.01	-0.01	-0.01	-0.02	-0.02
DF 30, 15, 3	0.37	0.38	0.37	0.36	0.37	0.38	0.39	0.38	0.37	0.38	0.38	0.38	0.38	0.38	0.38	0.38	0.38
DF 30, 30, 2	-0.06	-0.09	-0.11	-0.12	-0.12	-0.11	-0.09	-0.08	-0.07	-0.06	-0.06	-0.05	-0.05	-0.04	-0.03	-0.03	-0.03
DF 30, 30, 3	-0.29	-0.32	-0.37	-0.37	-0.40	-0.42	-0.45	-0.40	-0.38	-0.40	-0.36	-0.33	-0.35	-0.32	-0.28	-0.33	-0.34
DF 30, 60, 2	-0.40	-0.49	-0.57	-0.58	-0.51	-0.42	-0.33	-0.27	-0.23	-0.20	-0.18	-0.16	-0.14	-0.10	-0.08	-0.05	-0.02
DF 30, 60, 3	-0.26	-0.38	-0.40	-0.36	-0.36	-0.37	-0.45	-0.42	-0.36	-0.37	-0.35	-0.30	-0.31	-0.29	-0.31	-0.28	-0.28

Table 3: Unfiltered deposited fraction for final MT model measurements. DF x, y, z denotes inhaler inlet angle (which MT model), flow rate in l/min, APS ID. Particle sizes 1.8 to 5.8 μm.

Diameter (μm)	1.843	1.981	2.129	2.288	2.458	2.642	2.839	3.051	3.278	3.523	3.786	4.068	4.371	4.698	5.048	5.425	5.829
DF 0, 15, 2	-0.09	-0.07	-0.05	-0.03	-0.02	0.00	0.02	0.04	0.04	0.05	0.06	0.08	0.09	0.11	0.13	0.16	0.20
DF 0, 15, 3	-0.21	-0.23	-0.26	-0.28	-0.30	-0.32	-0.32	-0.31	-0.29	-0.24	-0.18	-0.10	-0.02	0.06	0.13	0.19	0.25
DF 0, 30, 2	0.02	0.05	0.08	0.11	0.14	0.18	0.20	0.20	0.20	0.23	0.27	0.31	0.35	0.39	0.43	0.48	0.53
DF 0, 30, 3	0.02	0.03	0.06	0.08	0.12	0.15	0.19	0.23	0.26	0.28	0.30	0.34	0.40	0.45	0.51	0.55	0.59
DF 0, 60, 2	-0.06	0.02	0.08	0.15	0.24	0.30	0.33	0.34	0.33	0.37	0.43	0.48	0.53	0.58	0.62	0.67	0.71
DF 0, 60, 3	0.48	0.49	0.50	0.51	0.53	0.55	0.57	0.58	0.59	0.60	0.62	0.65	0.70	0.73	0.74	0.76	0.80
DF 15, 15, 2	-0.02	-0.03	-0.05	-0.06	-0.07	-0.08	-0.09	-0.08	-0.08	-0.08	-0.07	-0.06	-0.04	-0.01	0.02	0.07	0.12
DF 15, 15, 3	0.26	0.26	0.26	0.26	0.26	0.26	0.26	0.25	0.24	0.23	0.22	0.24	0.28	0.31	0.34	0.38	0.41
DF 15, 30, 2	-0.03	-0.03	-0.03	-0.03	-0.02	-0.01	0.01	0.03	0.07	0.11	0.16	0.22	0.28	0.34	0.40	0.47	0.54
DF 15, 30, 3	0.26	0.25	0.26	0.27	0.27	0.28	0.31	0.33	0.34	0.36	0.39	0.44	0.50	0.56	0.61	0.65	0.69
DF 15, 60, 2	0.17	0.21	0.24	0.29	0.33	0.38	0.44	0.49	0.54	0.60	0.65	0.69	0.73	0.77	0.80	0.82	0.85
DF 15, 60, 3	0.43	0.44	0.45	0.47	0.49	0.51	0.53	0.55	0.56	0.59	0.65	0.70	0.76	0.81	0.84	0.87	0.88
DF 30, 15, 2	-0.03	-0.03	-0.04	-0.04	-0.04	-0.05	-0.05	-0.04	-0.03	-0.03	-0.01	0.01	0.05	0.09	0.15	0.23	0.30
DF 30, 15, 3	0.38	0.37	0.36	0.37	0.38	0.39	0.40	0.41	0.41	0.42	0.45	0.48	0.52	0.56	0.60	0.64	0.68
DF 30, 30, 2	-0.02	-0.02	-0.01	0.01	0.03	0.06	0.10	0.14	0.19	0.25	0.31	0.36	0.43	0.50	0.56	0.62	0.68
DF 30, 30, 3	-0.36	-0.35	-0.37	-0.36	-0.32	-0.28	-0.22	-0.14	-0.05	0.06	0.20	0.36	0.49	0.59	0.67	0.73	0.78
DF 30, 60, 2	0.02	0.07	0.13	0.19	0.26	0.34	0.41	0.48	0.54	0.60	0.65	0.69	0.73	0.76	0.79	0.82	0.84
DF 30, 60, 3	-0.35	-0.49	-0.62	-0.67	-0.68	-0.63	-0.51	-0.36	-0.18	0.04	0.27	0.49	0.65	0.72	0.78	0.83	0.87

Table 4: Unfiltered deposited fraction for final MT model measurements. DF x, y, z denotes inhaler inlet angle (which MT model), flow rate in l/min, APS ID. Particle sizes 6.2 to 10.4 μm.

Diameter (μm)	6.264	6.732	7.234	7.774	8.354	8.977	9.647	10.37
DF 0, 15, 2	0.24	0.30	0.36	0.43	0.49	0.56	0.63	0.70
DF 0, 15, 3	0.32	0.38	0.42	0.44	0.42	0.38	0.39	0.41
DF 0, 30, 2	0.59	0.66	0.72	0.78	0.83	0.87	0.89	0.89
DF 0, 30, 3	0.64	0.68	0.70	0.73	0.73	0.72	0.75	0.76
DF 0, 60, 2	0.75	0.79	0.83	0.86	0.89	0.91	0.93	0.94
DF 0, 60, 3	0.84	0.86	0.88	0.90	0.91	0.92	0.92	0.94
DF 15, 15, 2	0.19	0.29	0.37	0.44	0.53	0.56	0.60	0.66
DF 15, 15, 3	0.45	0.48	0.50	0.53	0.54	0.52	0.56	0.57
DF 15, 30, 2	0.60	0.67	0.74	0.79	0.81	0.78	0.72	0.67
DF 15, 30, 3	0.72	0.75	0.78	0.81	0.84	0.87	0.90	0.94
DF 15, 60, 2	0.87	0.88	0.88	0.87	0.83	0.78	0.68	0.54
DF 15, 60, 3	0.90	0.91	0.93	0.94	0.94	0.96	0.96	0.98
DF 30, 15, 2	0.38	0.48	0.57	0.65	0.70	0.71	0.71	0.61
DF 30, 15, 3	0.73	0.78	0.82	0.86	0.89	0.90	0.92	0.93
DF 30, 30, 2	0.73	0.78	0.82	0.86	0.88	0.89	0.88	0.86
DF 30, 30, 3	0.83	0.87	0.89	0.92	0.94	0.96	0.95	0.96
DF 30, 60, 2	0.86	0.88	0.90	0.91	0.92	0.93	0.92	0.92
DF 30, 60, 3	0.89	0.91	0.93	0.94	0.95	0.96	0.97	0.98